

A FAST FOURIER TRANSFORM APPROACH TO FINDING THE THICKNESS OF
SINGLE-LAYER THIN FILMS WITH SLOWLY VARYING INDICES OF
REFRACTION AND NEGLIGIBLE ABSORPTION COEFFICIENTS

THESIS

Presented to the Graduate Council of
Texas State University-San Marcos
in Partial Fulfillment
of the Requirements

for the Degree

Master of SCIENCE

by

Geoffrey F. Miller, B.S.

San Marcos, Texas
August 2012

A FAST FOURIER TRANSFORM APPROACH TO FINDING THE THICKNESS
OF SINGLE-LAYER THIN FILMS WITH SLOWLY VARYING INDICES OF
REFRACTION AND NEGLIGIBLE ABSORPTION COEFFICIENTS

Committee Members Approved:

Matthias Christoph Chung, Chair

Wilhelmus J. Geerts

Gregory B. Passty

Approved:

J. Michael Willoughby
Dean of the Graduate College

COPYRIGHT

by

Geoffrey F. Miller

2012

FAIR USE AND AUTHOR'S PERMISSION STATEMENT

Fair Use

This work is protected by the Copyright Laws of the United States (Public Law 94-553, section 107). Consistent with fair use as defined in the Copyright Laws, brief quotations from this material are allowed with proper acknowledgment. Use of this material for financial gain without the author's express written permission is not allowed.

Duplication Permission

As the copyright holder of this work I, Geoffrey F. Miller, authorize duplication of this work, in whole or in part, for educational or scholarly purposes only.

ACKNOWLEDGEMENTS

My research was made possible by the generous financial support of the National Science Foundation under grant DMR-0923506.

I would like to thank my committee members, Matthias C. Chung, Wilhelmus J. Geerts, and Gregory B. Passty, for their wonderful advice and encouragement.

I also owe special gratitude to the awesome administrative assistants in the math office, LaJuan Hallum, Melinda Guerrero, and BeKaye Keller—you are math-radical!

And, last but definitely not least, AMDG.

This manuscript was submitted on June 4, 2012.

TABLE OF CONTENTS

	Page
ACKNOWLEDGEMENTS	v
LIST OF TABLES	viii
LIST OF FIGURES	ix
ABSTRACT	x
CHAPTER	
I. MOTIVATION OF THE STUDY	1
General Background	1
Our Nonstandard Exposure Tool	1
Problem Statement	4
Plan of the Thesis	6
II. PHYSICAL THEORY OF THIN FILMS	7
Plan of the Chapter.....	7
Obtaining Reflectance Coefficients from Maxwell's Equations	7
The Refractive Index.....	7
Fresnel Equations for a Single-Layer Interface	9
Total Reflection Coefficient for a Two-Interface System	12
Calculating Thickness from the Periodicity of Reflectance Spectra	14
Locating Local Extrema.....	14
Calculating Thin Film Thickness from Local Extrema	15
Calculating Thin Film Thickness from Periodicity	16
III. DEVELOPING AN FFT ALGORITHM	18
Plan of the Chapter.....	18
Overview and Preliminaries	19
Definition of Fourier Series	19
Calculating Fourier Coefficients	20
Convergence of Fourier Series.....	23
Criterion for the Convergence of Fourier Series.....	23

Formula for the Sum of Cosines	24
Partial Sum of a Fourier Series	25
Pointwise and Uniform Convergence of a Fourier Series	26
DFT and the Cooley-Tukey FFT Algorithm.....	32
Discrete Fourier Transform.....	32
Inverse Discrete Fourier Transform.....	34
Fast Fourier Transform Algorithm of Cooley-Tukey	35
Pseudocode for the FFT Algorithm	36
IV. PROOF OF CONCEPT AND FURTHER RESEARCH	38
Plan of the Chapter.....	38
Implementation of an FFT algorithm in C++	41
Analysis of Simulated Data	43
Differing Film Thicknesses and Angles of Incident Light	43
Accounting for a Conical Spread in Incident Light	44
Noise Simulation.....	48
Preliminary Data and Conclusion	49
APPENDIX A: PHOTORESIST DATA	51
REFERENCES	58

LIST OF TABLES

Table	Page
1. Finding an Optimal Number of Data Points	40
2. Differing Film Thicknesses and Angles of Incident Light	44

LIST OF FIGURES

Figure	Page
1. Nonstandard Exposure Tool	2
2. Linewidth vs. Exposure Dose	5
3. Exposure Dose vs. Photoresist Thickness.....	5
4. Single-Interface Thin Film System.....	8
5. Boundary Conditions	10
6. Two-Interface Thin Film System.....	13
7. Noisy Sine Wave.....	18
8. Substrates and Reflectance	39
9. Sample Data File	40
10. Angle of Incidence and Reflectance	45
11. Beam Shaping and Beam Steering.....	47
12. Probability of an Acceptable Measurement	49
13. Preliminary Data	50

ABSTRACT

A FAST FOURIER TRANSFORM APPROACH TO FINDING THE THICKNESS OF
SINGLE-LAYER THIN FILMS WITH SLOWLY VARYING INDICES OF
REFRACTION AND NEGLIGIBLE ABSORPTION COEFFICIENTS

by

Geoffrey F. Miller, B.S.

Texas State University-San Marcos

August 2012

SUPERVISING PROFESSOR: MATTHIAS CHRISTOPH CHUNG

A nonstandard photolithographic exposure tool motivates the search for a method to determine photoresist thickness in real time. Optical physics of two-interface thin film systems and the theory of Fourier series reveal a way to calculate photoresist thickness by applying an FFT (fast Fourier transform) algorithm to the reflectance spectrum of a light beam incident on the photoresist. Analyses of simulated data and preliminary measurements assess the speed and accuracy of the FFT algorithm and suggest further areas of research.

CHAPTER I

MOTIVATION OF THE STUDY

General Background

Photolithography is a process that uses a chemical bath to selectively remove exposed or unexposed parts of a light-sensitive thin film layer, often called a photoresist, from a substrate material. In effect, the process involves writing patterns onto the photoresist via light, hence the etymology of the term "photolithography," which originates from the Greek φῶς (phos), which means light, λίθος (lithos), which means stone, and γράφειν (graphien), which means to write. Modified spaces in the photoresist left behind by the chemical bath permit the placement of diverse microstructures and nanostructures. Photolithographic processes thus play major roles in many modern industries, especially those concerned with the fabrication of integrated electronic circuits, magnetic devices such as hard disk drive heads, optical devices like those found in laser pointers, mechanical devices such as bubble jet printer components, and combinations of aforesaid technologies fundamental to the operation of liquid crystal displays and magnetic random access memory.

Our Nonstandard Exposure Tool

Standard exposure tools write projected patterns from stenciled masks onto a flat wafer covered by a uniform layer of photoresist, but they lack the depth of field needed to

treat non-uniform arrangements, such as those resulting from using a non-flat substrate.

The optical characterization laboratory at Texas State University-San Marcos is developing an exposure tool to perform photolithography on non-flat substrates. Such a tool would allow the combination of integrated optics, mechanics, and electronics in novel 3D devices. A schematic of the tool is depicted in Figure 1 below.

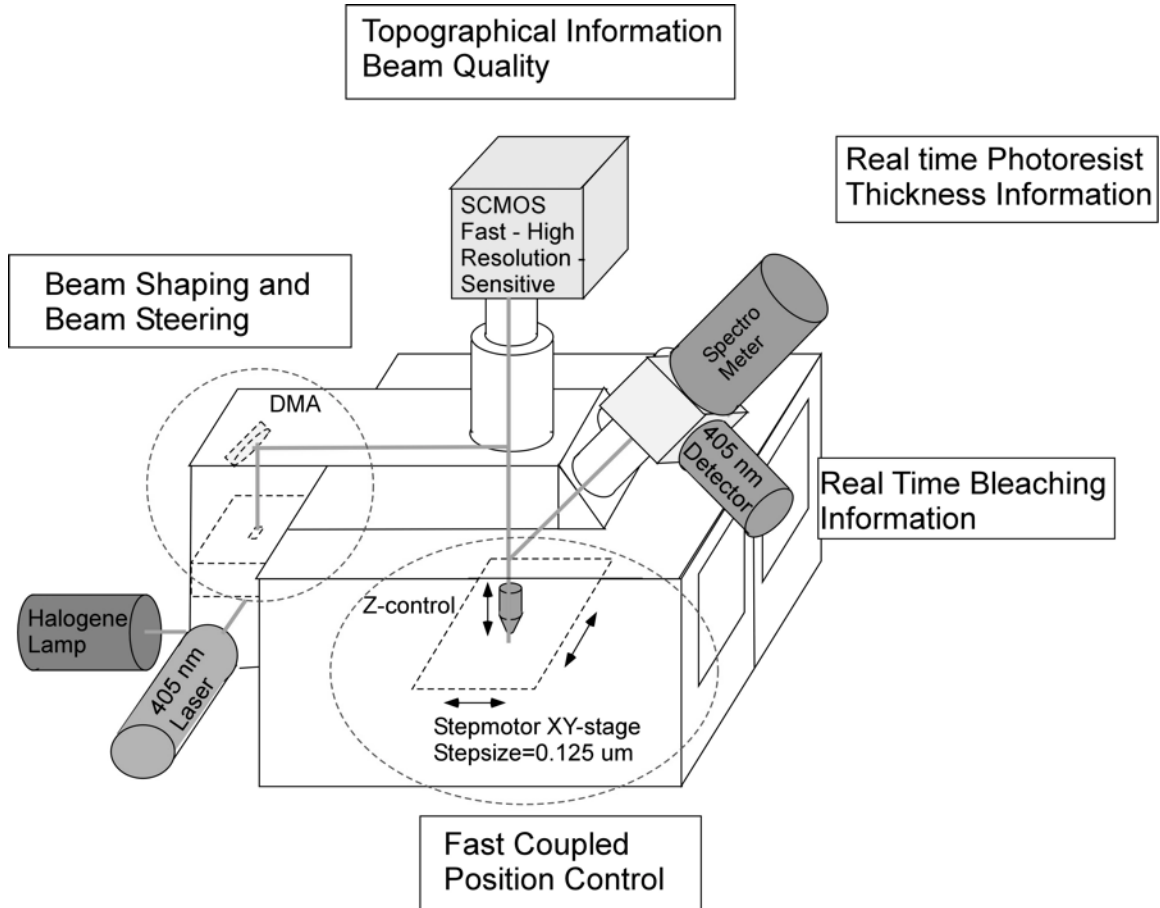


Figure 1. Nonstandard Exposure Tool. A 405 nm laser chemically alters portions of a non-uniform photoresist layer that is deposited on a substrate, which are subsequently removed in a chemical bath. The objective moves along the z-axis and the table positions the sample in the xy-plane.

We have chosen to use a positive photoresist, Shipley S1813, with our system, such that areas exposed to a proper amount of light at wavelength 405 nm will become soluble in developer chemicals. It is important to note that our photoresist has a negligible absorption coefficient and a slowly varying index of refraction. The meaning

and importance of these properties will be explained in the next chapter. Please refer to the datasheet in Appendix A for more detailed information about our photoresist.

Our apparatus is nonstandard and uses a laser to expose a sample situated on a movable table in the xy-plane, labeled "Fast Coupled Position Control" in Figure 1. The photons emitted by the laser are at a sufficiently high enough energy to chemically alter the photoresist. Focusing our laser is accomplished by adjusting the objective along the z-axis with a piezoelectric transducer that has fine control $\pm 50 \mu\text{m}$ and a step-motor that has coarse control $\pm 12 \text{ mm}$. Exposure is done without using a stenciled mask, instead inscribing the desired pattern directly onto the photoresist using the focused laser analogously to a pencil.

Other portions of our apparatus also require explanation. "Topographical Information" is used to move the objective along the z-axis to keep the sample in focus. The photons emitted from the filtered halogen lamp do not have a sufficient amount of energy to alter our photoresist. A dichroic beam splitter separates the reflected laser light beam (wavelength $\lambda = 405 \text{ nm}$) from the reflected halogen beam ($500 \text{ nm} < \lambda < 1000 \text{ nm}$). The reflected halogen beam is received into the fast spectrometer, labeled "Real Time Photoresist Thickness Information." We define the beam's reflectance spectrum as the square of the ratio of the norm of the amplitude of the reflected light waves to that of incident light waves at each wavelength in the beam. How to use the reflectance spectrum to determine photoresist thickness, and thus an appropriate photoresist exposure dosage of 405 nm light, will be the primary focus of our thesis. The instrument labeled "Real Time Bleaching Information" presents an alternative method to measure the required exposure dosage that is beyond the scope of our study. We will briefly touch upon the

components collectively labeled "Beam Shaping and Beam Steering" in the final chapter of our thesis.

Problem Statement

A photoresist layer deposited by a spinner on a flat wafer is rather homogeneous with slight variations in thickness near the edges; however, covering a non-flat substrate with photoresist using an eyedropper or airbrush will result in a non-homogeneous photoresist layer, with thickness conforming to surface topography. Photolithography on a substrate with unknown and variable photoresist layer thickness requires assessment of thin film depth at each point of exposure to ensure a correct dosage of light is given. Thus, for our exposure tool to work on arbitrary samples, it will be necessary to accurately measure the local thickness of the photoresist layer in real time and to correct the intensity of the laser or the speed of the movable table in the xy-plane accordingly.

Our accuracy goal is to calculate photoresist thickness within $\pm 6\%$ of the actual value. Our rationale stems from our apparatus' registration error, $\pm 0.125 \mu\text{m}$, in locating an exact x or y position on the xy-plane. For the patterns the laser writes, we want the line width error due to thin film thickness miscalculation to be less than this value, so referring to Figure 2, we find that our exposure dosage should be $165 \pm 30 \text{ mJ/cm}^2$. Referring to Figure 3, the allowable error in thickness estimation is therefore $\pm 6\%$.

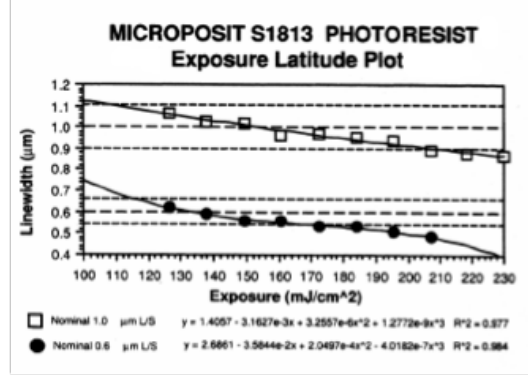


Figure 2. Linewidth vs. Exposure Dose. See Appendix A for original context.

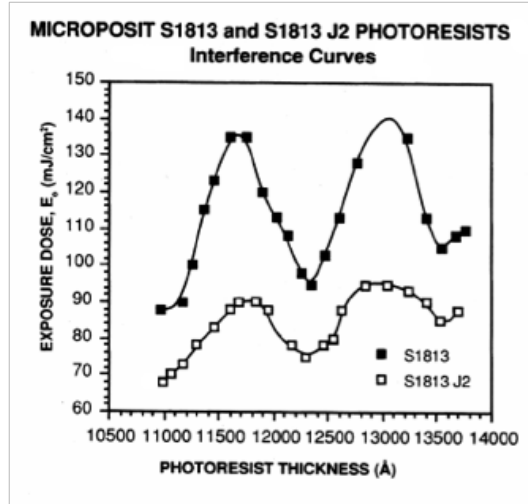


Figure 3. Exposure Dose vs. Photoresist Thickness. See Appendix A for original context.

The justification for our time goal of less than one millisecond comes from the fact that we can only write one pixel per millisecond due to the constraints imposed by the intensity of our laser. To write our patterns as efficiently as possible, we need to finish the thickness calculation in less than this amount of time so that for every pixel we can determine the photoresist thickness and thus determine the required exposure dosage.

Plan of the Thesis

In the next chapter, we will review relevant optical principles and discuss how the physical properties of our Shipley S1813 photoresist permit us to calculate thickness from the periodicity of a reflectance spectrum for a beam of light containing wavelengths beyond the range of those that can chemically alter our thin film.

In the third chapter, we will present the general theory of Fourier series, explain why a Fourier series expansion of the modeling equation for a reflectance spectrum is legitimate, and explain how a fast Fourier transform can find the approximate periodicity of a reflectance spectrum.

In the final chapter, we will use Film WizardTM from SCI (Scientific Computing International) to generate simulated reflectance spectra for differing substrates, angles of incident light, thin film thicknesses, and intensities of white noise to emulate the noise present in measurements obtained by our exposure tool. We will analyze our results in light of the goals set in our problem statement, discuss relevant optical features of our apparatus, and suggest further areas of research as well as critique the utility of our simulations for predicting the behavior of data obtained using our apparatus. We will also look at some preliminary measurement data for our photoresist on a SiN substrate.

CHAPTER II

PHYSICAL THEORY OF THIN FILMS

Plan of the Chapter

As mentioned in the previous chapter, the optical properties of our photoresist will suggest a method of calculating the thin film's thickness from its reflectance spectrum.

In the first section, we will review the law of refraction, derive the Fresnel coefficients at a single interface using Maxwell's equations, and finally construct a modeling equation for the reflectance spectrum of a single-layer thin film system involving two interfaces. In the second section, we will calculate thin film thickness from the periodicity of our modeling equation.

Obtaining Reflectance Coefficients from Maxwell's Equations

The Refractive Index

Light travels at different speeds through different materials. When light passes from one medium to another, this change in speed results in a change in direction. We call this phenomenon refraction and define the refractive index n of a given material as the speed of light in a vacuum divided by the speed of light in the material. Snell's Law governs refraction, where the angles of incidence θ_a and refraction θ_f are related by

$$\frac{\sin\theta_a}{\sin\theta_f} = \frac{n_f}{n_a}, \quad [\text{II.1}]$$

where n_a and n_f refer to the refractive indices for the respective media (the subscript a refers to the ambient, the subscript f refers to the single-layer thin film, and the subscript s , which has not been used yet, refers to the substrate). Another portion of light is reflected at an angle $\theta_r = \theta_a$. Figure 4 illustrates the situation.

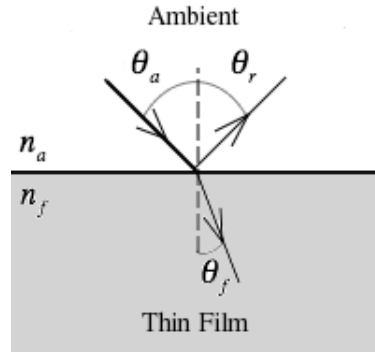


Figure 4. Single-Interface Thin Film System. A beam of light is incident at the interface of an ambient and thin film.

Most materials also absorb some of the light that passes through them. We can thus speak of a complex index of refraction, $\tilde{N} = n - ik$, where n is the refractive index previously defined, i is the imaginary number, and k is the extinction coefficient; the extinction coefficient is related to α , the absorption coefficient, by $\alpha = \frac{4\pi k}{\lambda}$, where λ refers to the wavelength of incident light. Snell's Law still holds for this new quantity (Tompkins and McGahan 1999, 220). However, dielectrics have negligible absorption coefficients and our substrates, such as Si and SiN, and thin film, Shipley S1813 photoresist, behave like dielectrics for light wavelengths above 500 nm. We may thus assume that we are only dealing with the real number version of the refractive index.

Moreover, because the refractive indices of our photoresist and substrate are slowly varying, we may consider n_f and n_s constant over the domain 500 nm to 1000 nm.

Fresnel Equations for a Single-Layer Interface

We are ultimately working toward finding an equation to model the reflectance spectrum, so we will start by finding the Fresnel reflection/transmission coefficients at a planar single-layer interface like that depicted in Figure 4.

Let us define the plane of incidence to be parallel to the page. We can distinguish four distinct amplitudes for the incident light wave: the electric field component E_a^{\parallel} parallel to the plane of incidence, the electric field component E_a^{\perp} perpendicular to the plane of incidence, and the magnetic field components B_a^{\parallel} and B_a^{\perp} , which are defined analogously. Similarly, we have E_r^{\parallel} , E_r^{\perp} , B_r^{\parallel} , and B_r^{\perp} for the reflected light wave and E_f^{\parallel} , E_f^{\perp} , B_f^{\parallel} , and B_f^{\perp} for the transmitted light wave. Our Fresnel coefficients are

$$\begin{aligned} r_{\parallel} &= \frac{E_r^{\parallel}}{E_a^{\parallel}}, & r_{\perp} &= \frac{E_r^{\perp}}{E_a^{\perp}}, \\ t_{\parallel} &= \frac{E_t^{\parallel}}{E_a^{\parallel}}, & t_{\perp} &= \frac{E_t^{\perp}}{E_a^{\perp}}. \end{aligned} \quad [\text{II.2}]$$

We wish to express the ratios of [II.2] in terms of refractive indices and angles of incidence and transmission only. Graphical construction methods that utilize certain boundary conditions for electric and magnetic waves are possible (Doyle 1980, 646). However, in our opinion, Maxwell's equations offer a more insightful and intuitive way to derive the aforementioned boundary conditions and thus the desired form of [II.2].

We turn in particular to the integral forms of Gauss' law for electric fields and magnetism, Faraday's law, and Ampere's law, which are listed below, in order; note that ϵ_0 refers to the vacuum permittivity and μ_0 refers to the vacuum permeability, also

known as the electric and magnetic constants, respectively (Jackson 1999, 2, 16-17). If any other symbols seem unfamiliar, do not worry; we will explain our notation as we discuss the boundary conditions for each equation.

$$\int_S \epsilon_0 \vec{E} \cdot d\hat{A} = \int_V \rho dV, \quad [\text{II.3a}]$$

$$\int_S \vec{B} \cdot d\hat{A} = 0, \quad [\text{II.3b}]$$

$$\oint_{\Gamma} \vec{E} \cdot d\hat{s} = -\frac{d\Phi_B}{dt}, \quad [\text{II.3c}]$$

$$\oint_{\Gamma} \frac{\vec{B}}{\mu_0} \cdot d\hat{s} = \int \vec{J} \cdot d\hat{A} + \epsilon_0 \frac{d\Phi_E}{dt}. \quad [\text{II.3d}]$$

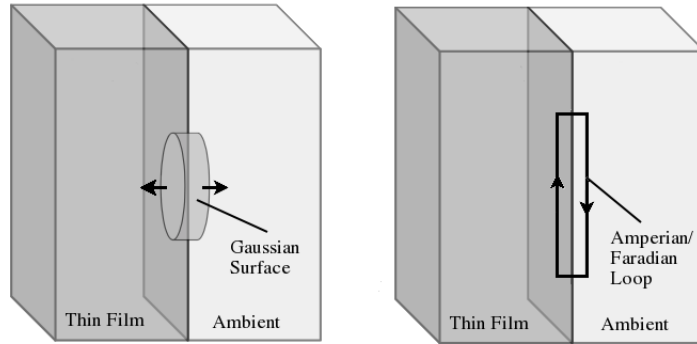


Figure 5. Boundary Conditions. A Gaussian surface and an Amperian/Faradian loop are positioned across the single-layer interface. These imaginary geometric constructs are used to determine boundary conditions for Maxwell's equations.

Equations [II.3a] and [II.3b] are area integrals taken over a Gaussian surface S that is positioned across the single-layer interface, as pictured in Figure 5. Note that our charge density $\rho = 0$ throughout the volume V contained by our Gaussian surface. By letting the thickness of our surface approach zero and noticing that \vec{B} and \vec{E} are perpendicular to each other and perpendicular to the direction of wave propagation, i.e.

$\bar{B} = n \hat{k} \times \bar{E}$, where \hat{k} is a unit vector pointing in the direction of the light wave's propagation, we get our first two boundary conditions,

$$\begin{aligned} 0 &= \int_S \epsilon_0 \bar{E} \cdot d\hat{A} = E_a^{\parallel} \cos \theta_a + E_r^{\parallel} \cos \theta_r - E_f^{\parallel} \cos \theta_f \\ \therefore (E_a^{\parallel} - E_r^{\parallel}) \cos \theta_a &= E_f^{\parallel} \cos \theta_f, \end{aligned} \quad [\text{II.4}]$$

$$\begin{aligned} 0 &= \int_S \bar{B} \cdot d\hat{A} = B_a^{\parallel} \cos \theta_a - B_r^{\parallel} \cos \theta_r - B_f^{\parallel} \cos \theta_f \\ \therefore n_a (E_a^{\perp} - E_r^{\perp}) \cos \theta_a &= n_f E_f^{\perp} \cos \theta_f. \end{aligned}$$

Equations [II.3c] and [II.3d] are line integrals along an Amperian/Faradian loop Γ that is positioned across the single-layer interface, as pictured in Figure 5. By letting the width of our loop approach zero, we reduce the magnetic and electric fluxes through the loop (Φ_B and Φ_E , respectively) to zero; the flow of current through the loop, $\int \bar{J} \cdot d\hat{A}$, also goes to zero. We thus obtain our last two boundary conditions,

$$\begin{aligned} 0 &= \oint_{\Gamma} \bar{E} \cdot d\hat{s} = E_a^{\perp} + E_r^{\perp} - E_f^{\perp} \\ \therefore E_a^{\perp} + E_r^{\perp} &= E_f^{\perp}, \end{aligned} \quad [\text{II.5}]$$

$$\begin{aligned} 0 &= \oint_{\Gamma} \frac{\bar{B}}{\mu_0} \cdot d\hat{s} = B_a^{\perp} + B_r^{\perp} - B_f^{\perp} \\ \therefore n_a (E_a^{\perp} + E_r^{\perp}) &= n_f E_f^{\perp}. \end{aligned}$$

Algebraic manipulation of our boundary conditions in [II.4] and [II.5] yields the desired forms of the Fresnel coefficients,

$$\begin{aligned} r^{\parallel} &= \frac{n_f \cos \theta_a - n_a \cos \theta_f}{n_f \cos \theta_a + n_a \cos \theta_f}, & r^{\perp} &= \frac{n_a \cos \theta_a - n_f \cos \theta_f}{n_a \cos \theta_a + n_f \cos \theta_f}, \\ t^{\parallel} &= \frac{2n_a \cos \theta_a}{n_f \cos \theta_a + n_a \cos \theta_f}, & t^{\perp} &= \frac{2n_a \cos \theta_a}{n_a \cos \theta_a + n_f \cos \theta_f}. \end{aligned} \quad [\text{II.6}]$$

Total Reflection Coefficient for a Two-Interface System

Our thin film lies on a substrate, and due to repeated internal reflections, we must use the Fresnel coefficients at two distinct interfaces to formulate a total reflection coefficient for the whole system. To simplify calculations, we introduce a new notation: each Fresnel coefficient will be labeled with an ordered pair of subscript letters indicating the interface in question and the direction in which light waves are propagating. For example, $r_{af}^{\parallel} = \frac{n_f \cos \theta_a - n_a \cos \theta_f}{n_f \cos \theta_a + n_a \cos \theta_f}$ refers to the reflection coefficient for light waves traveling from the ambient to the thin film, polarized parallel to the plane of incidence. Thus, suppose we consider light waves traveling from medium x to medium y . Then from [II.6] we have

$$\begin{aligned} r_{xy}^{\parallel} &= \frac{n_y \cos \theta_x - n_x \cos \theta_y}{n_y \cos \theta_x + n_x \cos \theta_y}, & r_{xy}^{\perp} &= \frac{n_x \cos \theta_x - n_y \cos \theta_y}{n_x \cos \theta_x + n_y \cos \theta_y}, \\ t_{xy}^{\parallel} &= \frac{2n_x \cos \theta_x}{n_y \cos \theta_x + n_x \cos \theta_y}, & t_{xy}^{\perp} &= \frac{2n_x \cos \theta_x}{n_x \cos \theta_x + n_y \cos \theta_y}. \end{aligned} \quad [\text{II.7}]$$

To find the total reflection coefficient, we must consider the contributions of internal reflections that are partially transmitted back into the ambient. Our system is depicted below in Figure 6.

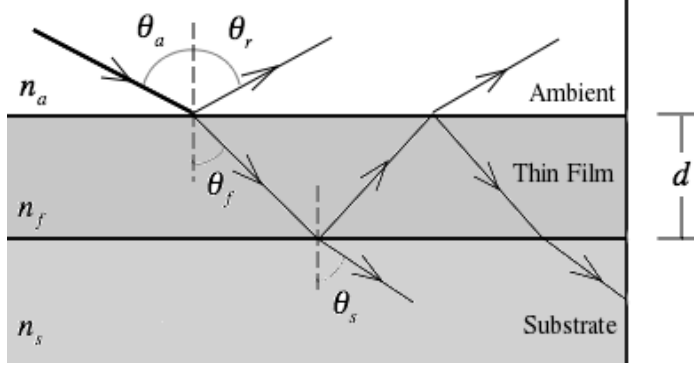


Figure 6. Two-Interface Thin Film System. A beam of light travels through a two-interface thin film system and undergoes internal reflection within the thin film layer.

When light waves are first incident at the surface of the thin film, reflected waves of either orientation to the plane of incidence are reflected back with r_{af} times the amplitude of the original waves incident on the sample. The waves transmitted at the ambient-film interface will partly reflect at the film-substrate interface; after one internal reflection at the film-substrate interface, waves at $t_{af}r_{fs}t_{fa}e^{-i2\beta}$ times the amplitude of the incident waves will escape back into the ambient; etc. We must also take into account a phase shift,

$$\beta = 2\pi \left(\frac{d}{\lambda} \right) n_f \cos \theta_f, \quad [\text{II.8}]$$

incurred by the wave while traveling through the thin film, where d denotes thin film thickness and λ denotes the wavelength of the incident light waves (Tompkins and McGahan 1999, 19). Note that our photoresist has negligible absorption for $\lambda > 500$ nm, so n_f and θ_f are real, whence β is real. The process of internal reflection and partial transmission back into the ambient carries on indefinitely. Thus, our total reflection coefficient is given by the series

$$\begin{aligned} R &= r_{af} + t_{af}t_{fa}r_{fs}e^{-i2\beta} + t_{af}t_{fa}r_{fa}r_{fs}^2e^{-i4\beta} + t_{af}t_{fa}r_{fa}^2r_{fs}^3e^{-i6\beta} + \dots \\ &= r_{af} + t_{af}t_{fa}r_{fs}e^{-i2\beta} \left[1 + r_{fa}r_{fs}e^{-i2\beta} + (r_{fa}r_{fs}e^{-i2\beta})^2 + \dots \right]. \end{aligned} \quad [\text{II.9}]$$

However, recall the well-known identity,

$$\frac{1}{1-x} = 1 + x + x^2 + x^3 + x^4 + \dots, \quad x^2 < 1. \quad [\text{II.10}]$$

If we set $x = r_{fa}r_{fs}e^{-i2\beta}$, we may thus write

$$R = r_{af} + \frac{t_{af}t_{fa}r_{fs}e^{-i2\beta}}{1 - r_{fa}r_{fs}e^{-i2\beta}}. \quad [\text{II.11}]$$

We can further simplify our expression by observing that [II.7] implies

$$\begin{aligned} r_{yx} &= -r_{xy}, \\ t_{yx} &= \frac{1 - r_{xy}^2}{t_{xy}}. \end{aligned} \quad [\text{II.12}]$$

Therefore, we obtain

$$R = \frac{r_{df} + r_{fs}e^{-i2\beta}}{1 + r_{af}r_{fs}e^{-i2\beta}}. \quad [\text{II.13}]$$

Again, all that we have said in this section holds for light polarized either parallel to or perpendicular to the plane of incidence. That is why we have left off the superscripts \parallel and \perp in our notation. Reflectance \mathfrak{R} is defined simply as the square of the norm of the total reflection coefficient given by [II.13]. This is the expression we have been seeking to model our reflectance spectrum.

Calculating Thickness from the Periodicity of Reflectance Spectra

Locating Local Extrema

Because reflectance \mathfrak{R} is defined relative to [II.13], we have the following proportionality relation between \mathfrak{R} and RR^* ,

$$\Re \propto RR^* = \frac{(r_{af} + r_{fs} \exp(-i2\beta))(r_{af} + r_{fs} \exp(i2\beta))}{(1 + r_{af}r_{fs} \exp(-i2\beta))(1 + r_{af}r_{fs} \exp(i2\beta))} =$$

$$\frac{r_{af}^2 + r_{fs}^2 + r_{af}r_{fs}(\exp(-i2\beta) + \exp(i2\beta))}{1 + r_{af}^2r_{fs}^2 + r_{af}r_{fs}(\exp(-i2\beta) + \exp(i2\beta))} = \frac{r_{af}^2 + r_{fs}^2 + r_{af}r_{fs}2\cos(2\beta)}{1 + r_{af}^2r_{fs}^2 + r_{af}r_{fs}2\cos(2\beta)}. \quad [\text{II.14}]$$

Note that because of the negligible absorption of light by our photoresist and substrate, we have assumed that r_{af} and r_{fs} are real. We observe that RR^* is a function of β , which is in turn a function of λ . Taking the derivative of [II.14] with respect to λ will thus give us the local extrema of reflectance spectra for two-interface systems where each medium

has a negligible absorption coefficient. Setting $\frac{d(RR^*)}{d\lambda} = 0$, we find

$$\frac{4\beta r_{af}r_{fs}(r_{af}^2 - 1)(r_{fs}^2 - 1)\sin(2\beta)}{\lambda(1 + r_{af}^2r_{fs}^2 + 2r_{af}r_{fs}\cos(2\beta))^2} = 0. \quad [\text{II.15}]$$

Therefore, [II.14] will exhibit local extrema whenever $\beta = m\frac{\pi}{2}, m \in \mathbb{Z}$. It follows that maxima (resp. minima) will occur every π units in β . Again, note that in the derivation of [II.15], we assumed that our photoresist and substrate have negligible absorption and that the optical properties of the photoresist and substrate are not dependent on wavelength.

Calculating Thin Film Thickness from Local Extrema

Let λ_m and λ_{m+1} be wavelengths at adjacent maxima (resp. minima) on the reflectance spectrum. It follows that,

$$\begin{aligned}
m\pi &= 2\pi \left(\frac{d}{\lambda_m} \right) n_f \cos \theta_f, & (m+1)\pi &= 2\pi \left(\frac{d}{\lambda_{m+1}} \right) n_f \cos \theta_f, \\
m &= \frac{2dn_f}{\lambda_m} \cos \theta_f, & m+1 &= \frac{2dn_f}{\lambda_{m+1}} \cos \theta_f
\end{aligned}
\tag{II.16}$$

$$\begin{aligned}
\left(\frac{2dn_f}{\lambda_{m+1}} - \frac{2dn_f}{\lambda_m} \right) \cos \theta_f &= (m+1) - m = 1 \\
2dn_f (\lambda_m - \lambda_{m+1}) \cos \theta_f &= \frac{\lambda_m \lambda_{m+1}}{\lambda_m \lambda_{m+1}} \\
d &= \frac{2n_f (\lambda_m - \lambda_{m+1}) \cos \theta_f}{2n_f (\lambda_m - \lambda_{m+1}) \cos \theta_f}.
\end{aligned}$$

In terms of photon energy measured in eV, we obtain

$$d = \frac{\hbar c}{2n_f (E_{m+1} - E_m) \cos \theta_f}, \tag{II.17}$$

where $E = \frac{\hbar c}{\lambda}$, $\hbar c \approx 1240 \text{ eV} \cdot \text{nm}$.

Calculating Thin Film Thickness from Periodicity

The advantage of expression [II.17] is that when reflectance is plotted against photon energy, local extrema are equally spaced (Tompkins and McGahan 1999, 59). This means that the thickness of the thin film can be determined from the periodicity of the reflectance spectrum, which may be calculated from the maximum mode of the corresponding discrete Fourier spectrum as detailed in Chapter III. For now, suffice it to say that if we denote the dominant periodicity by ρ , we may rewrite [II.17] as

$$d = \frac{\hbar c}{2n_f \rho \cos \theta_f}. \tag{II.18}$$

Equation [II.18] remains valid for reflectance spectra of light waves with arbitrary polarization or even random polarization, since any light wave can be expressed as the linear superposition of component waves polarized parallel to and perpendicular to the plane of incidence (Sakurai and Napolitano 2011, 6-8). Equation [II.18] certainly holds

for these two basic polarizations of light, and if the functions $R_{\parallel}R_{\parallel}^*$ and $R_{\perp}R_{\perp}^*$ each have a periodicity ρ , then the function $RR^* = w_{\parallel}R_{\parallel}R_{\parallel}^* + w_{\perp}R_{\perp}R_{\perp}^*$, where w_{\parallel} and w_{\perp} are appropriate constants, must also have a periodicity ρ .

CHAPTER III

DEVELOPING AN FFT ALGORITHM

Plan of the Chapter

In the previous chapter, we found that the thickness of a thin film can be determined from the periodicity ρ of its corresponding reflectance spectrum, provided that certain physical conditions are met.

We could calculate ρ by scrolling linearly through the data and picking out local extrema, then doubling the average distance between them. However, noise is inherent in measurements, and will not afford us such a simple solution. Consider, for instance, a sine wave with 10% white noise, sampled at 50 equidistant points. Looking at Figure 7, it is hard to intuit a scheme that could scroll through the data linearly, toss out all the spurious local extrema introduced by the "spikes," and yet keep the actual local extrema.

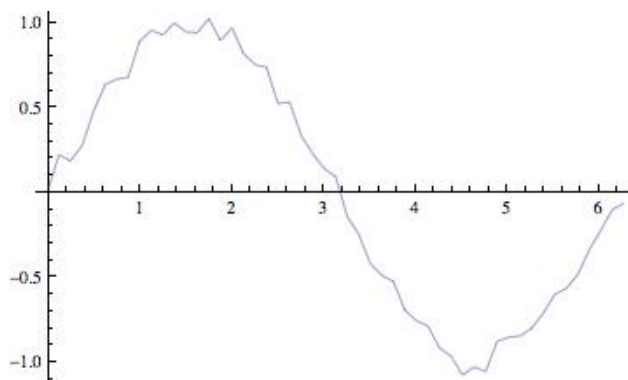


Figure 7. Noisy Sine Wave. A sine wave sampled at 50 equidistant points, with 10% random noise.

A better approach is to use what is called a discrete Fourier transform to construct an approximation of the original function from a linear superposition of exponential functions. The periodicity of the original function can then be estimated from the weights of the superposition, as we shall explain in a later section.

We will start our discussion with an example. The following *Mathematica* 7 code uses a discrete Fourier transform to find the periodicity of our simple sine function with 10% white noise as depicted in Figure 7.

```
In[1]:= data = Table[Sin[x] + RandomReal[{-0.1, 0.1}], {x, 0, 2 Pi, 2 Pi/50}];
f = Rest[Abs[Fourier[data]]];
pos = Position[f, Max[f]][[1, 1]];
2 Pi/pos
Out[4]= 2 π
```

Notice that the output gives the correct period. Chapter III of our thesis boils down to explaining how and why the above code snippet works.

Before we can talk more about discrete Fourier transforms, we must define what Fourier series are and discuss what kind of functions can be expanded as Fourier series.

Overview and Preliminaries

Definition of Fourier Series

Suppose a function $f(x)$ has the period 2τ and can be expanded as

$$f(x) = \frac{a_0}{2} + \sum_{n=1}^{\infty} \left[a_n \cos\left(\frac{\pi n}{\tau} x\right) + b_n \sin\left(\frac{\pi n}{\tau} x\right) \right], \quad [\text{III.1}]$$

where a_n, b_n are constants. We call this expansion the Fourier series for $f(x)$. With an

appropriate substitution of variables, $x = \frac{\tau}{\pi} t$, we can transform [III.1] into a function of

periodicity 2π , and vice versa. Thus, from hereon out, we shall assume that all our functions are periodic on an interval of 2π , $[0, 2\pi]$, whence [III.1] becomes simply

$$f(x) = \frac{a_0}{2} + \sum_{n=1}^{\infty} (a_n \cos nx + b_n \sin nx). \quad [\text{III.2}]$$

We will also assume that all such functions are integrable, unless specified otherwise; we require this to calculate our Fourier coefficients, a_n, b_n , in the next section.

Using Euler's formula, $e^{ix} = \cos x + i \sin x$, we can rewrite our Fourier series in terms of the exponential basis, $\{e^{inx}\}$, as follows:

$$f(x) = \sum_{n=-\infty}^{\infty} c_n e^{inx}, \quad c_n = \begin{cases} \frac{1}{2}(a_n - ib_n) & , \quad n > 0, \\ \frac{1}{2}a_0 & , \quad n = 0, \\ \frac{1}{2}(a_{-n} + ib_{-n}) & , \quad n < 0. \end{cases} \quad [\text{III.3}]$$

For some applications, such as determining the maximum mode of a frequency spectrum, it is easier to work with [III.3]. In our opinion, however, many properties of Fourier series are more intuitively established using [III.2], since complex functions are harder to visualize. We will thus be alternating between the two representations.

Calculating Fourier Coefficients

To calculate the Fourier coefficients, a_n, b_n , we will exploit the orthogonality of the trigonometric basis. An infinite collection of functions $\{\varphi_i\}$ is said to be orthogonal provided that the following conditions are satisfied, where i, j are non-negative integers such that $i \neq j$ and the symbol * denotes the complex conjugate,

$$\int_0^{2\pi} \varphi_i(x) \varphi_j^*(x) dx = 0 \quad \text{and} \quad [\text{III.4}]$$

$$\int_0^{2\pi} \varphi_i(x) \varphi_i^*(x) dx \neq 0.$$

Proposition 1: The trigonometric basis, $\{1, \cos x, \sin x, \cos 2x, \sin 2x, \dots\}$, is orthogonal.

Proof: For any integer $n \neq 0$, we have $\int_0^{2\pi} \cos nx dx = 0$ and $\int_0^{2\pi} \sin nx dx = 0$. We

observe the following,

$$\int_0^{2\pi} \cos^2 nx dx = \int_0^{2\pi} \frac{1+2\cos nx}{2} dx = \pi, \quad [\text{III.5}]$$

$$\int_0^{2\pi} \sin^2 nx dx = \int_0^{2\pi} \frac{1-2\cos nx}{2} dx = \pi.$$

Moreover, for another integer $m \neq n$, we have

$$\int_0^{2\pi} \cos nx \cos mx dx = \frac{1}{2} \int_0^{2\pi} [\cos(n+m)x + \cos(n-m)x] dx = 0,$$

$$\int_0^{2\pi} \sin nx \sin mx dx = \frac{1}{2} \int_0^{2\pi} [\cos(n-m)x - \cos(n+m)x] dx = 0, \quad [\text{III.6}]$$

$$\int_0^{2\pi} \sin nx \cos mx dx = \frac{1}{2} \int_0^{2\pi} [\sin(n+m)x + \sin(n-m)x] dx = 0.$$

This completes the proof. \square

Corollary 1: The exponential basis, $\{e^{inx}\}$, is orthogonal.

Proof: Since $e^{inx} = \cos nx + i \sin nx$, this follows from Proposition 1. \square

To find a_0 , we integrate both sides of [III.2] over the interval $[0, 2\pi]$. We obtain

$$\begin{aligned} \int_0^{2\pi} f(x) dx &= \frac{a_0}{2} \int_0^{2\pi} dx + \sum_{n=1}^{\infty} \left(a_n \int_0^{2\pi} \cos nx dx + b_n \int_0^{2\pi} \sin nx dx \right) \\ &= \pi a_0. \end{aligned} \quad [\text{III.7}]$$

To find a_m (resp. b_m), $m > 0$, we return to our modified equation [III.1] and multiply both sides by $\cos mx$ (resp. $\sin mx$), and integrate as before. From Proposition 1, we obtain

$$\begin{aligned} \int_0^{2\pi} f(x) \cos mx dx &= \frac{a_0}{2} \int_0^{2\pi} \cos mx dx \\ &\quad + \sum_{n=1}^{\infty} \left(a_n \int_0^{2\pi} \cos nx \cos mx dx \right. \\ &\quad \left. + b_n \int_0^{2\pi} \sin nx \cos mx dx \right) \\ &= a_m \int_0^{2\pi} \cos^2 mx dx = a_m \pi, \end{aligned} \quad [\text{III.8}]$$

$$\begin{aligned} \int_0^{2\pi} f(x) \sin mx dx &= \frac{a_0}{2} \int_0^{2\pi} \sin mx dx \\ &\quad + \sum_{n=1}^{\infty} \left(a_n \int_0^{2\pi} \cos nx \sin mx dx \right. \\ &\quad \left. + b_n \int_0^{2\pi} \sin nx \sin mx dx \right) \\ &= b_m \int_0^{2\pi} \sin^2 mx dx = b_m \pi. \end{aligned}$$

The complex Fourier coefficients, c_n , are determined similarly,

$$c_n = \frac{1}{2\pi} \int_0^{2\pi} f(x) e^{-inx} dx. \quad [\text{III.9}]$$

Convergence of Fourier Series

Criterion for the Convergence of Fourier Series

Now that we know what a Fourier series is, we may tackle the question of what functions have Fourier series expansions, and in particular, whether one exists for the model of our reflectance spectrum, [II.14]. This leads to the criterion for the convergence of Fourier series, which obliges us to introduce some new vocabulary. First, we state the theorem, then, we will provide the definitions.

Main Theorem: The Fourier series of a function $f(x)$ that is smooth on $[0,2\pi]$ converges absolutely and uniformly to $f(x)$ for all values of $x \in (0,2\pi)$.

We say that a function is smooth on an interval if the function is everywhere differentiable. It is easy to see that every smooth function is continuous. By absolute and uniform convergence, we mean the usual definitions found in introductory analysis textbooks, or more intuitively, that our original function can be approximated to arbitrary closeness by taking only a finite number of terms from its Fourier expansion.

Our model for the reflectance spectrum, [II.14], satisfies the conditions of our Main Theorem if we remember the physical constraint $r_{xy} \in (0,1)$. Expression [II.14] can be made to have a period of 2π by an appropriate substitution of variables as was done for [III.1] and is everywhere differentiable by [II.15]. All that remains is to prove our Main Theorem.

We shall follow Tolstov's outline of proof, but rearranging, subtracting, and adding material as we think is best for our application, which does not require all the

machinery he develops (Tolstov 1976, 66-82). Our strategy will be to find an integral expression for the first k terms of a Fourier series, denoted by $S_k(x)$, and then to use this expression to prove that equality holds in [III.1] for a smooth function $f(x)$. We will next demonstrate the absolute and uniform convergence of the Fourier series, and this will complete our proof.

Formula for the Sum of Cosines

We begin by proving a lemma and noting a corollary.

$$\text{Lemma 1: } \frac{1}{2} + \cos x + \cos 2x + \cdots + \cos nx = \frac{\sin\left[x\left(n + \frac{1}{2}\right)\right]}{2\sin\left(\frac{x}{2}\right)}.$$

Proof: Let $S = \frac{1}{2} + \cos x + \cos 2x + \cdots + \cos nx$. It follows that

$$2S \sin \frac{x}{2} = \sin \frac{x}{2} + 2\cos x \sin \frac{x}{2} + 2\cos 2x \sin \frac{x}{2} + \cdots + 2\cos nx \sin \frac{x}{2}. \quad [\text{III.10}]$$

Applying the trigonometric identity $2\cos \alpha \sin \beta = \sin(\alpha + \beta) - \sin(\alpha - \beta)$, the right hand side of [III.10] becomes

$$\begin{aligned} & \sin \frac{x}{2} + \left(\sin \frac{3x}{2} - \sin \frac{x}{2} \right) + \left(\sin \frac{5x}{2} - \sin \frac{3x}{2} \right) + \\ & \cdots + \left\{ \sin \left[x \left(n + \frac{1}{2} \right) \right] - \sin \left[x \left(n - \frac{1}{2} \right) \right] \right\} = \sin \left[x \left(n + \frac{1}{2} \right) \right] \end{aligned} \quad [\text{III.11}]$$

Dividing both sides of [III.10] by $2\sin \frac{x}{2}$, we obtain our desired identity. \square

Corollary 2: The following identity holds, $\frac{1}{\pi} \int_0^{2\pi} \frac{\sin\left[x\left(n + \frac{1}{2}\right)\right]}{2\sin\left(\frac{x}{2}\right)} dx = 1.$

Proof: From Lemma 1, we have

$$\begin{aligned} \frac{1}{\pi} \int_0^{2\pi} \frac{\sin\left[x\left(n + \frac{1}{2}\right)\right]}{2\sin\left(\frac{x}{2}\right)} dx &= \frac{1}{\pi} \int_0^{2\pi} \left(\frac{1}{2} + \cos x + \cos 2x + \cdots + \cos nx \right) dx \\ &= \frac{1}{\pi} \int_0^{2\pi} \frac{1}{2} dx + \cdots + \frac{1}{\pi} \int_0^{2\pi} \cos nx dx \\ &= \frac{1}{\pi} \int_0^{2\pi} \frac{1}{2} dx = 1. \end{aligned} \quad [\text{III.12}]$$

Note that the integral of $\cos nx$ over $[0, 2\pi]$ vanishes for any nonzero integer n because we are working with a function of even symmetry on the interval. \square

Partial Sum of a Fourier Series

Suppose we take only the first k terms of a Fourier series,

$$S_k(x) = \frac{a_0}{2} + \sum_{n=1}^k (a_n \cos nx + b_n \sin nx). \quad [\text{III.13}]$$

Substituting the expressions for our Fourier coefficients from [III.7] and [III.8], we obtain

$$\begin{aligned} S_k(x) &= \frac{1}{2\pi} \int_0^{2\pi} f(t) dt + \\ &\quad \frac{1}{\pi} \sum_{n=1}^k \left[\left(\int_0^{2\pi} f(t) \cos nt dt \right) \cos nx + \left(\int_0^{2\pi} f(t) \sin nt dt \right) \sin nx \right] \\ &= \frac{1}{\pi} \int_0^{2\pi} f(t) \left[\frac{1}{2} + \sum_{n=1}^k (\cos nt \cos nx + \sin nt \sin nx) \right] dt \\ &= \frac{1}{\pi} \int_0^{2\pi} f(t) \left\{ \frac{1}{2} + \sum_{n=1}^k \cos[n(t - x)] \right\} dt. \end{aligned} \quad [\text{III.14}]$$

Lemma 1 then allows us to write

$$\begin{aligned} S_k(x) &= \frac{1}{\pi} \int_0^{2\pi} f(t) \left\{ \frac{1}{2} + \sum_{n=1}^k \cos[n(t-x)] \right\} dt \\ &= \frac{1}{\pi} \int_0^{2\pi} f(t) \frac{\sin\left[(t-x)\left(k+\frac{1}{2}\right)\right]}{2\sin\left(\frac{t-x}{2}\right)} dt. \end{aligned} \quad [\text{III.15}]$$

To simplify our notation, we set $u = t - x$ and notice that both $f(t) = f(x+u)$ and

$\frac{\sin\left[u\left(k+\frac{1}{2}\right)\right]}{2\sin\left(\frac{u}{2}\right)}$ have a period of 2π , whence their product also has a period of 2π . This

means that $S_k(x)$ will have a fixed value for fixed k as long as our integral is taken over an interval of length 2π . Therefore,

$$S_k(x) = \frac{1}{\pi} \int_0^{2\pi} f(x+u) \frac{\sin\left[u\left(k+\frac{1}{2}\right)\right]}{2\sin\left(\frac{u}{2}\right)} du. \quad [\text{III.16}]$$

We call [III.16] the integral formula for the partial sum of a Fourier series. Expression

[III.16] will assist in proving that $\lim_{k \rightarrow \infty} S_k(x) = f(x)$.

Pointwise and Uniform Convergence of a Fourier Series

We are now in a position to prove that $f(x)$ can be approximated on $(0, 2\pi)$ by taking the first k terms of its Fourier series. We will show the pointwise convergence of the series and then prove uniform and absolute convergence, which will allow us to say with certainty that for all $\varepsilon > 0$, there exists a positive k such that $|S_k(x) - f(x)| < \varepsilon$ on the appropriate interval. We start with some lemmas.

Lemma 2: Let $f(x)$ be continuous on $[a,b]$. Then, for all $\varepsilon > 0$, there exists a continuous, piecewise smooth function $g(x)$ such that $|f(x) - g(x)| < \varepsilon$, $x \in [a,b]$.

Proof: Let $\varepsilon > 0$. Because $[a,b]$ is closed and bounded, $f(x)$ is uniformly continuous on the interval. Thus, there exists $\delta > 0$ such that $|x - y| < \delta$ implies

$|f(x) - f(y)| < \frac{\varepsilon}{2}$. Choose a partition $\{x_i\}_0^n$ of $[a,b]$ such that $x_{i+1} - x_i < \delta$. Define a

function $g(x)$ on $[a,b]$ such that $g(x) = \frac{f(x_{i+1}) - f(x_i)}{x_{i+1} - x_i}(x - x_i) + f(x_i)$ on each

subinterval $[x_i, x_{i+1}]$. We note that $g(x)$ is a continuous, piecewise smooth function.

Moreover,

$$\begin{aligned} |f(x) - g(x)| &= \left| f(x) - \left[\frac{f(x_{i+1}) - f(x_i)}{x_{i+1} - x_i}(x - x_i) + f(x_i) \right] \right| \\ &\leq |f(x) - f(x_i)| + \left| \frac{f(x_{i+1}) - f(x_i)}{x_{i+1} - x_i}(x - x_i) \right| \\ &< \frac{\varepsilon}{2} + \frac{\varepsilon/2}{\delta} \cdot \delta = \varepsilon. \end{aligned} \quad [\text{III.17}]$$

This completes the proof. \square

Lemma 3: Let $f(x)$ be continuous on $[a,b]$. Then, for all $\varepsilon > 0$, there exists a

continuous, piecewise smooth function $g(x)$ such that $\int_a^b |f(x) - g(x)| dx < \varepsilon$.

Proof: From Lemma 2, we know there exists a continuous, piecewise smooth function $g(x)$ such that $|f(x) - g(x)| < \frac{\varepsilon}{b-a}$. It follows that

$$\int_a^b |f(x) - g(x)| dx < \int_a^b \frac{\varepsilon}{b-a} dx = \varepsilon. \quad \square$$

Lemma 4: Let $f(x)$ be continuous on $[a,b]$. Then, $\lim_{p \rightarrow \infty} \int_a^b f(x) \sin px dx = 0$.

Proof: Let $\epsilon > 0$. According to Lemma 3, there exists a continuous, piecewise smooth function $g(x)$ such that $\int_a^b |f(x) - g(x)| dx < \frac{\epsilon}{2}$. We observe

$$\begin{aligned} \left| \int_a^b f(x) \sin px dx \right| &= \left| \int_a^b [f(x) - g(x) + g(x)] \sin px dx \right| \\ &\leq \int_a^b |f(x) - g(x)| dx + \left| \int_a^b g(x) \sin px dx \right|. \end{aligned} \quad [\text{III.18}]$$

Note that $\int_a^b g(x) \sin px dx = -\frac{1}{p} [g(x) \cos px]_a^b - \frac{1}{p} \int_a^b g'(x) \sin px dx$. Thus, for sufficiently

large p , $\left| \int_a^b g'(x) \sin px dx \right| < \frac{\epsilon}{2}$. This means that $\left| \int_a^b f(x) \sin px dx \right| < \epsilon$, or in other words,

$$\lim_{p \rightarrow \infty} \int_a^b f(x) \sin px dx = 0 \text{ is true. } \square$$

Theorem 1: Let $f(x)$ be a smooth function on $[0, 2\pi]$. Then, $\lim_{k \rightarrow \infty} S_k(x) = f(x)$ is true for all $x \in [0, 2\pi]$.

Proof: We want to show that $\lim_{k \rightarrow \infty} \frac{1}{\pi} \int_0^{2\pi} f(x+u) \frac{\sin \left[u \left(k + \frac{1}{2} \right) \right]}{2 \sin \left(\frac{u}{2} \right)} du = f(x)$. The

identity established in Corollary 2 gives $f(x) = \frac{1}{\pi} \int_0^{2\pi} f(x) \frac{\sin \left[u \left(k + \frac{1}{2} \right) \right]}{2 \sin \left(\frac{u}{2} \right)} du$, which

reduces our proof to verifying that

$$\lim_{k \rightarrow \infty} \frac{1}{\pi} \int_0^{2\pi} [f(x+u) - f(x)] \frac{\sin \left[u \left(k + \frac{1}{2} \right) \right]}{2 \sin \left(\frac{u}{2} \right)} du = 0. \quad [\text{III.19}]$$

First, define $\Phi(u) = \frac{f(x+u) - f(x)}{2 \sin \left(\frac{u}{2} \right)} = \frac{f(x+u) - f(x)}{u} \cdot \frac{u}{2 \sin \left(\frac{u}{2} \right)}$ and set $\Phi(0) = \lim_{u \rightarrow 0} \Phi(u)$.

We know that $\lim_{u \rightarrow 0} \frac{f(x+u) - f(x)}{u}$ exists because $f(x)$ is smooth on $[0, 2\pi]$. Also,

$\lim_{u \rightarrow 0} \frac{u}{2 \sin u} = \frac{1}{2}$. It follows that $\Phi(u)$ continuous. According to Lemma 4, we have that

$$\lim_{k \rightarrow \infty} \frac{1}{\pi} \int_0^{2\pi} \Phi(u) \sin \left[u \left(k + \frac{1}{2} \right) \right] du = 0, \text{ which verifies [III.19]. } \square$$

Now that we have demonstrated pointwise convergence, we proceed with establishing absolute and uniform convergence. Suppose we are given a smooth function $f(x)$ on $[0, 2\pi]$ that has a Fourier series expansion of the form [III.2]. We consider the following lemmas.

Lemma 5: The series $\sum_{n=1}^{\infty} (a_n^2 + b_n^2)$ converges, where a_n, b_n are the Fourier coefficients as defined in [III.8].

Proof: Switching to the complex representation of the Fourier series in [III.3] and keeping in mind the orthogonality of exponential functions as shown in Corollary 1, we observe

$$\begin{aligned}
0 &\leq \int_0^{2\pi} \left[f(x) - \sum_{n=-\infty}^{\infty} c_n e^{inx} \right]^2 dx \\
&= \int_0^{2\pi} f^2(x) dx - 2 \sum_{n=-\infty}^{\infty} c_n \int_0^{2\pi} f(x) e^{inx} dx + \sum_{n=-\infty}^{\infty} c_n^2 \int_0^{2\pi} e^{2inx} dx \\
&= \int_0^{2\pi} f^2(x) dx - 2 \sum_{n=-\infty}^{\infty} c_n \int_0^{2\pi} f(x) e^{inx} dx \\
&\leq \int_0^{2\pi} f^2(x) dx - \sum_{n=-\infty}^{\infty} c_n^2.
\end{aligned} \tag{III.20}$$

This implies $\int_{-\pi}^{\pi} f^2(x) dx \geq \left(\frac{a_0}{2}\right)^2 + \sum_{n=1}^{\infty} (a_n^2 + b_n^2)$, whence $\sum_{n=1}^{\infty} (a_n^2 + b_n^2)$ converges. \square

Lemma 6: The series $\sum_{n=1}^{\infty} (|a_n| + |b_n|)$ converges, where a_n, b_n are the Fourier coefficients as

defined in [III.8].

Proof: Using integration by parts, we have

$$\begin{aligned}
a_n &= \int_0^{2\pi} f(x) \cos nx dx \\
&= \frac{1}{\pi n} \left[f(x) \sin nx \right]_0^{2\pi} - \frac{1}{\pi n} \int_0^{2\pi} f'(x) \sin nx dx \\
&= -\frac{1}{\pi n} \int_0^{2\pi} f'(x) \sin nx dx = -\frac{b'_n}{n},
\end{aligned} \tag{III.21}$$

$$\begin{aligned}
b_n &= \int_0^{2\pi} f(x) \sin nx dx \\
&= -\frac{1}{\pi n} \left[f(x) \cos nx \right]_0^{2\pi} + \frac{1}{\pi n} \int_0^{2\pi} f'(x) \cos nx dx \\
&= \frac{1}{\pi n} \int_0^{2\pi} f'(x) \cos nx dx = \frac{a'_n}{n},
\end{aligned}$$

where a'_n, b'_n are the Fourier coefficients for $f'(x)$. Note that

$$\begin{aligned} \left(|a'_n| - \frac{1}{n} \right)^2 &= a'^2_n - \frac{2|a'_n|}{n} + \frac{1}{n^2} \geq 0, \\ \left(|b'_n| - \frac{1}{n} \right)^2 &= b'^2_n - \frac{2|b'_n|}{n} + \frac{1}{n^2} \geq 0. \end{aligned} \quad [\text{III.22}]$$

Algebraic manipulation of [III.22] gives $\frac{|a'_n|}{n} + \frac{|b'_n|}{n} \leq \frac{1}{2}(a'^2_n + b'^2_n) + \frac{1}{n^2}$. The series

$\sum_{n=1}^{\infty} (a'^2_n + b'^2_n)$ converges by Lemma 5. $\sum_{n=1}^{\infty} \frac{1}{n^2}$ converges as well because it is a geometric

series. It follows that $\sum_{n=1}^{\infty} \left(\frac{|a'_n|}{n} + \frac{|b'_n|}{n} \right)$ converges. Substituting [III.21] gives that

$\sum_{n=1}^{\infty} (|a_n| + |b_n|)$ converges, which completes the proof. \square

Theorem 2: Let $f(x)$ be a continuous, smooth function on $[0, 2\pi]$. Then, the Fourier series of $f(x)$ converges absolutely and uniformly.

Proof: It suffices to show that the series $\sum_{n=1}^{\infty} (|a_n \cos nx| + |b_n \sin nx|)$ converges.

Noting that the trigonometric functions are bounded below by -1 and above by 1 , we observe $|a_n \cos nx| + |b_n \sin nx| \leq |a_n| + |b_n|$. Therefore, our result follows from Lemma 6. \square

Main Theorem: The Fourier series of a smooth function $f(x)$ that is continuous on $[0, 2\pi]$ converges absolutely and uniformly to $f(x)$ for all values of $x \in (0, 2\pi)$.

Proof: Our Main Theorem is an immediate consequence of Theorems 1 and 2. \square

DFT and the Cooley-Tukey FFT Algorithm

We will not discuss the theory behind discrete Fourier transforms (DFTs) with the same rigor as we discussed the convergence of Fourier series, seeing as how they are approximations thereof. Instead, we will focus on their applications and properties, particularly those that are directly relevant to ascertaining the periodicity ρ of our reflectance spectrum. We rely primarily on Sauer and Vogel, but have made alterations and clarifications to their presentations (Sauer 2006, 475-477; Vogel 2002, 64-68).

Discrete Fourier Transform

Suppose that we can only sample a smooth function $f(x)$ at a finite sequence of points $\{x_j\}_0^{n-1}$ on $[0, 2\pi]$ satisfying $x_j = j \frac{2\pi}{n}$, where n is even. In this case, our discretization of $f(x)$ in vector notation is

$$\mathbf{f} = \begin{bmatrix} f_0 \\ f_1 \\ \vdots \\ f_{n-1} \end{bmatrix}, \quad f_j = f(x_j). \quad [\text{III.23}]$$

Because we only have n data points, we cannot find a unique, infinite Fourier series to fit our data. In fact, infinitely many distinct infinite Fourier series will fit our sampling. To see why, add to $f(x)$ another continuous, smooth function $g(x)$ that is not everywhere zero but is zero at each x_j . The Fourier series expansions for $f(x)$, $g(x)$, and $f(x) + g(x)$ are obviously distinct, but each fits the sequence of points $\{f(x_j)\}_0^{n-1}$. This phenomenon is known as aliasing.

Instead, we seek an approximate, finite Fourier series of the form

$$f_j = \sum_{k=0}^{n-1} c_k e^{ikx_j}, \quad [\text{III.24}]$$

where the c_k 's are constants yet to be determined. Taking advantage of the equidistant spacing of our x_j 's, we can rewrite [III.24] as

$$f_j = \sum_{k=0}^{n-1} c_k e^{2\pi i k j / n}. \quad [\text{III.25}]$$

To simplify our notation further, let $\omega = \omega_n = e^{2\pi i / n}$ and $\omega_m = e^{2\pi i / m}$ for any nonzero integer m . Expression [III.25] becomes

$$f_j = \sum_{k=0}^{n-1} c_k \omega^{jk}. \quad [\text{III.26}]$$

Equation [III.26] is known as the discrete Fourier transform (DFT) of $f(x)$ on n points.

To see how our transform can give the periodicity of the original function, it is helpful to write [III.26] in matrix notation.

$$\begin{bmatrix} 1 & 1 & 1 & \dots & 1 \\ 1 & \omega & \omega^2 & \dots & \omega^{n-1} \\ 1 & \omega^2 & \omega^4 & \dots & \omega^{2(n-1)} \\ \vdots & \vdots & \vdots & \ddots & \vdots \\ 1 & \omega^{n-1} & \omega^{2(n-1)} & \dots & \omega^{(n-1)^2} \end{bmatrix} \begin{bmatrix} c_0 \\ c_1 \\ c_2 \\ \vdots \\ c_{n-1} \end{bmatrix} = \begin{bmatrix} f_0 \\ f_1 \\ f_2 \\ \vdots \\ f_{n-1} \end{bmatrix}. \quad [\text{III.27}]$$

The matrix \mathbf{F} is referred to as the Fourier matrix of order n . Observe that the k th column of \mathbf{F} , called a Fourier basis vector, is merely the discretization of the function ω^k over the interval $[0, n]$. The periodicity of ω^k is n/k . We are expressing \mathbf{f} as a linear superposition of the Fourier basis vectors with weights c_k . Therefore, the periodicity of \mathbf{f} can be approximated from that of the basis vector with the greatest weight by multiplying

the periodicity of said vector by $\frac{2\pi}{n}$ to return to the original domain over which $f(x)$

was sampled. Note that c_k might take on complex values, so we must consider $|c_k|$ to determine the greatest weight.

So far, we have assumed that $f(x)$ has been sampled on the interval $[0, 2\pi]$. We can, in fact, perform a DFT to find the periodicity of $f(x)$ sampled on any generic interval $[a, b]$. We simply treat the function as having been sampled on $[0, 2\pi]$, and then after determining the vector with the greatest weight, multiply the periodicity of said vector by $\frac{b-a}{n}$.

Inverse Discrete Fourier Transform

We now turn our discussion to how to calculate the weights, c_k . To calculate c_k , we use the inverse discrete Fourier transform (IDFT),

$$c_k = \frac{1}{n} \sum_{j=0}^{n-1} f_j \omega^{-kj}. \quad [\text{III.28}]$$

Equation [III.28] follows from a very convenient property of exponential functions. In Corollary 1, we proved orthogonality for exponential functions over the interval $[0, 2\pi]$. It can be shown that exponential functions are also orthogonal over a finite series of points $\left\{x_j\right\}_0^{n-1}$ on $[0, 2\pi]$ satisfying $x_j = j \frac{2\pi}{n}$, where n is even; we simply replace the integral with a sum (Arfken 914).

Consider the matrix $\mathbf{F}^* \mathbf{F}$, where \mathbf{F}^* is the matrix whose elements are the complex conjugate of those of \mathbf{F}^* . Denote the element in the j th row and k th column by $(\mathbf{F}^* \mathbf{F})_{jk}$.

We observe that

$$\begin{aligned}
(\mathbf{F}^* \mathbf{F})_{jk} &= \sum_{h=0}^{n-1} \omega^{-jh} \omega^{kh} \\
&= \sum_{h=0}^{n-1} e^{2\pi i h(k-j)/n} \\
&= n \delta_{jk},
\end{aligned} \tag{III.29}$$

whence $\mathbf{F}^* \mathbf{F} = n \mathbf{I}$, where \mathbf{I} denotes the $n \times n$ identity matrix. Thus, we have that

$F^{-1} = \frac{1}{n} F^*$, which allows us to rewrite [III.27] as $\mathbf{c} = \frac{1}{n} \mathbf{F}^* \mathbf{f}$ or [III.28].

Because we are interested only in comparing $|c_k|$ for our application, we may omit multiplication by $\frac{1}{n}$ from [III.28] and treat our IDFT as

$$c_k = \sum_{j=0}^{n-1} f_j \omega^{-kj}. \tag{III.30}$$

Our expression in [III.30] has the advantage of eliminating some unnecessary floating-point operations in computer implementations of the IDFT.

Fast Fourier Transform Algorithm of Cooley-Tukey

If n , the number of points sampled, is a power of 2, we can reduce the number of multiplications required to calculate [III.27] from n^2 to $n \log_2 n$ by exploiting the symmetry of the Fourier matrix, \mathbf{F} .

Returning to [III.28], let $m = \frac{n}{2}$ and observe that

$$\begin{aligned}
f_j &= \sum_{k=0}^{n-1} c_k \omega_n^{jk} = \sum_{k=0}^{m-1} \left(c_{2k} \omega_n^{2jk} + c_{2k+1} \omega_n^{(2j+1)k} \right) \\
&= \sum_{k=0}^{m-1} c_{2k} \omega_m^{jk} + \omega_m^k \sum_{k=0}^{m-1} c_{2k+1} \omega_m^{jk}.
\end{aligned} \tag{III.31}$$

Define $\tilde{f}_j^{\text{even}} = \sum_{k=0}^{m-1} c_{2k} \omega_m^{jk}$ and $\tilde{f}_j^{\text{odd}} = \sum_{k=0}^{m-1} c_{2k+1} \omega_m^{jk}$. We can repeat the procedure in [III.31] on each of $\tilde{f}_j^{\text{even}}$ and \tilde{f}_j^{odd} , and continue on recursively until we can no longer do so. At the bottom level, we will have n single-point DFTs, the solutions to which can be back-substituted until we reach the top.

At each level of our recursive procedure, notice that $\omega_m^{km} = e^{2\pi i k/m} = 1$, $k \in \mathbb{Z}$. This leads to the following relationships, where $0 \leq j < m$.

$$\begin{aligned}\tilde{f}_{m+j}^{\text{even}} &= \sum_{k=0}^{m-1} c_{2k} (\omega_m^{km}) \omega_m^{jk} = \tilde{f}_j^{\text{even}}, \\ \tilde{f}_{m+j}^{\text{odd}} &= \sum_{k=0}^{m-1} c_{2k+1} (\omega_m^{km}) \omega_m^{jk} = \tilde{f}_j^{\text{odd}}.\end{aligned}\quad [\text{III.32}]$$

Note that $\omega_n^m = e^{\pi i} = -1$ implies $\omega_n^{m+j} = -\omega_n^j$. Therefore, [III.31] and [III.32] lead to

$$\begin{aligned}f_j &= \tilde{f}_j^{\text{even}} + \omega_n^j \tilde{f}_j^{\text{odd}}, \\ f_{m+j} &= \tilde{f}_j^{\text{even}} - \omega_n^j \tilde{f}_j^{\text{odd}}.\end{aligned}\quad [\text{III.33}]$$

We now have all the essential elements of the fast Fourier transform (FFT) algorithm of Cooley-Tukey. A pseudocode implementation of the algorithm will assist comprehension of the abstract mathematical description just given, and so we will conclude the chapter with such an implementation.

Pseudocode for the FFT Algorithm

FFT(data[n], trans[n]) provides a recursive version of the Cooley-Tukey fast Fourier transform algorithm. The vector of sampled values of $f(x)$ is denoted by data[] and is assumed to have length n , where n is a power of 2. Results are stored in the transform vector, trans[]. To refer to the j th element of data[], we write data[j]. Value assignment will be denoted by $:=$, such that $x := 4$ means x now has the value 4. To

declare a new vector of length m , we write `vectorname[m]`. The construction of our conditional statements and loops follow common conventions.

```

FFT(data[], trans[])
  if (n = 1), let trans[0] := data[0];
  else, do the following
     $\omega_n := e^{2\pi i/n};$ 
    evenIndices[n/2];
    evenTrans[n/2];
    oddIndices[n/2];
    oddTrans[n/2];
    for (j := 0; j <  $\frac{n}{2}$ ; j++)
      evenIndices[j] := data[2j];
      oddIndices[j] := data[2j+1];
      FFT(evenIndices[], evenTrans[]);
      FFT(oddIndices[], oddTrans[n]);
    for (j := 0; j <  $\frac{n}{2}$ ; j++)
      trans[j] := evenTrans[j] +  $\omega_n^j$  oddTrans[j];
      trans[j +  $\frac{n}{2}$ ] := evenTrans[j] -  $\omega_n^j$  oddTrans[j];

```

CHAPTER IV

PROOF OF CONCEPT AND FURTHER RESEARCH

Plan of the Chapter

We will use data generated by Scientific Computing International's Film Wizard™ software to test the Cooley-Tukey FFT algorithm developed in the prior chapter. Film Wizard™ is a software package that can be used to calculate the reflection spectrum of a thin film or multilayer system. The software uses a database of previous professional measurements and the Fresnel reflection equations to generate spectra. Because the Film Wizard™ spectra do not contain noise, various degrees of white noise were added to the calculated spectra using Wolfram *Mathematica* 7 to emulate the noise we might expect from our apparatus. We define white noise as a noise parameter independent of wavelength and with identical amplitude across the reflectance spectrum.

The optical properties of Shipley S1813 photoresist for light above 500 nm are well approximated by those of SiO₂. We will use Al for our substrate in all trials unless otherwise noted. As Figure 8 demonstrates, using different substrates does not affect the periodicity of the reflectance spectrum provided that the substrates in question exhibit negligible dispersion of light; therefore, our choice of substrate is irrelevant for the purposes of testing our FFT algorithm as long as this criterion is met.

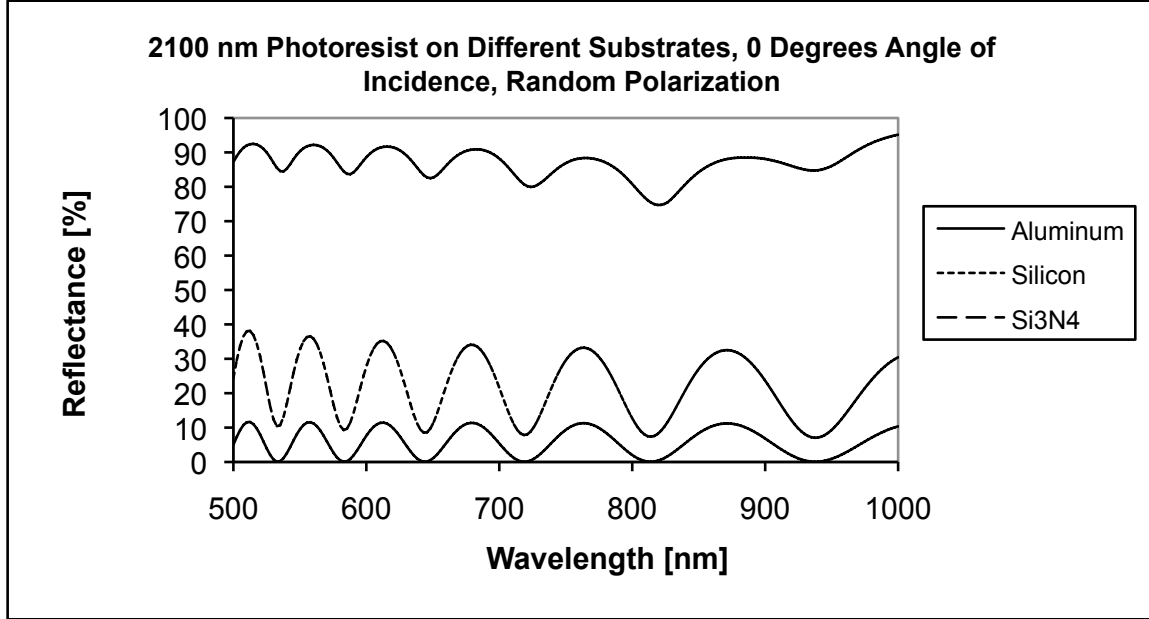


Figure 8. Substrates and Reflectance. Although the amplitude and constant component of the reflectance spectra are affected by changing the substrate, the spacing of extrema remains unaltered. Hence, the above spectra exhibit the same periodicity and predict the same thickness for our photoresist.

Our simulated reflectance spectra will consist of values taken at $n = 256$ equidistant points in the domain, which starts at photon energy 1.2398 eV (1000 nm) and ends at 2.4796 eV (500 nm). We have chosen $n = 256$ due to the fact that this number will meet our accuracy and time constraints for the FFT algorithm execution, as mentioned in the introduction, and also give the best trade-off between accuracy. The Ocean Optics HR2000+ES Spectrometer of our exposure tool in fact provides 1138 equidistant data points over the domain, spaced at 0.439 nm, on which we can perform a moving average to reduce noise and compress our total number of data points, using spline interpolations if necessary, to conform to the simulated model given by Film Wizard™. For a discussion of spline interpolations, refer to Schatzman. Table 1 illustrates how $n \geq 512$ violates our time constraint of 1 ms and how $n \leq 128$ does not give optimum accuracy. Recall that n must always be a power of 2 for the FFT algorithm

given in Chapter III. For the trials below, film thickness was set at 12000 nm and the angle of incident light was set at 30° . 100 trials were taken for each value of n .

Table 1. Finding an Optimal Number of Data Points.

Number of Data Points (n)	Average Execution Time (μs)	Measured Thickness (nm)	Percent Error (%)
64	78.82	10963.10	8.64
128	191.36	12424.90	3.54
256	468.45	12059.40	0.495
512	1128.40	12059.40	0.495

Concerning the method of our data analysis, reflectance data will be inputted to a C++ implementation of the aforementioned FFT algorithm via a single-column plain text file, a snippet of which is shown in Figure 9.

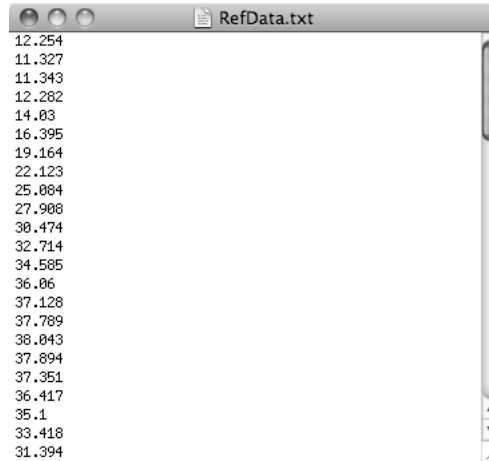


Figure 9. Sample Data File. The single-column text file RefData.txt stores reflectance spectrum percentage values. The domain is implied by the way in which we sample these values and so is not explicitly stated in the file.

As mentioned in Chapter I, during our data analysis we will vary the thickness of the thin film, the angle of incident light, and the intensity of white noise. The first section in this present chapter will state and explain the annotated C++ code used for the data analysis, while the analysis itself will occupy the second section alongside relevant discussions of certain optical components in our apparatus and suggested areas of further research. We will also provide some critiques of the utility of our simulations and preliminary measurements obtained by our exposure tool.

Implementation of an FFT algorithm in C++

For the sake of saving space, we omit portions of our source code that record calculation time and that facilitate file processing for data analysis, giving only those parts necessary to compute thin film thickness from a single input file. Many of our variables are hardcoded, so for the following C++ source, we have set the angle of incident light to 0 radians and the number of data points n to 256; these values must be changed manually based on the data contained in RefData.txt. The reader, however, may choose to handle file input/output differently should he or she adapt the code.

```
#include <iostream>
#include <cstdio>
#include <complex>
#include <cmath>
#include <fstream>
#define PI 3.14159
using namespace std;
typedef complex<double> dcomp;

/* FFT implements a recursive version of the Cooley-Tukey fast Fourier transform algorithm. The array of original values, data[], should not be modified. Results are stored in the transform array, trans[]. The integer value n refers to the size of both arrays, which must always be a power of 2. */

void FFT(const dcomp data[], dcomp trans[], int n);
```

```

/* FindMax is rather self-explanatory, except it works with the norms
of complex values. Also, because we are analyzing a Fourier spectrum,
the second half will be a repeat of the first half of the array, so we
needn't worry about it. We only go up to n/2. The first entry of the
array is the DC component of the frequency, which tells us nothing
about the dominant periodicity, so we ignore it. */

int FindMax(dcomp array[], int n);

int main()
{
    ifstream refData("RefData.txt");
    int datumNum = 256;                                // Datum in above file.
    dcomp data[datumNum];                            // Holds data.
    dcomp trans[datumNum];                           // Holds Fourier transform.
    double angle = asin(sin(0)/1.45691);           // Angle of refracted light

    /* Read data in from an appropriate text file. */
    if(refData.good())
    {
        int k = 0;
        while(!refData.eof() && k < datumNum)
        {
            refData >> data[k];
            k++;
        }
    }
    refData.close();

    /* Perform FFT. */
    FFT(data, trans, datumNum);
    int maxpos = FindMax(trans, datumNum);

    /* Compute Thin Film Thickness with [I.17] */
    double thickness = (1.98645 / pow(10., 25.)) / (1.45691 *
                                                    cos(angle) * datumNum / maxpos * 1.2398 /
                                                    datumNum * (1.602 / pow(10., 19.))) * 1 / 2;

    cout << "Thin Film Thickness: " << thickness * pow(10., 9) << endl;
}
void FFT(const dcomp data[], dcomp trans[], int n)
{
    if(n == 1)
    {
        trans[0] = data[0];      // The FFT of a single point is itself.
    }
    else
    {
        dcomp Wn = dcomp(cos(2 * PI / n), sin(2 * PI / n));

        /* Split data by even and odd indices, then FFT both parts. */
        dcomp evenIndices[n/2];
        dcomp evenTrans[n/2];
        dcomp oddIndices[n/2];
        dcomp oddTrans[n/2];
    }
}

```

```

        for(int i = 0; i < n/2; i++)
        {
            evenIndices[i] = data[2*i];
            oddIndices[i] = data[2*i + 1];
        }

        FFT(evenIndices, evenTrans, n/2);
        FFT(oddIndices, oddTrans, n/2);
        /* Construct the transform, using a recursive relationship. */
        for(int i = 0; i < n/2; i++)
        {
            trans[i] = evenTrans[i] + pow(Wn, i) * oddTrans[i];
            trans[i+n/2] = evenTrans[i] - pow(Wn, i) * oddTrans[i];
        }
    }

    int FindMax(dcomp array[], int n)
    {
        int max = 1;
        double maxNorm = norm(array[1]);
        for(int i = 1; i < n/2; i++)
        {
            if(maxNorm < norm(array[i + 1]))
            {
                max = i + 1;
                maxNorm = norm(array[max]);
            }
        }
        return max;
    }
}

```

Analysis of Simulated Data

Differing Film Thicknesses and Angles of Incident Light

We tested our algorithm with light incident at $\theta_a = 0,15^\circ, 30^\circ$ for thin film thicknesses 3000 nm, 6000 nm, 12000 nm. Our reason for choosing these angles is that they are good representatives for the angular spread in the focused light beam emitted by our exposure tool. Our chosen thicknesses represent a range we might expect from Shipley S1813 photoresist deposited on a non-flat substrate material. No white noise was included in these trials, since we wished to focus only on the effects of varying θ_a . Table 2 displays our results.

Table 2. Differing Film Thicknesses and Angles of Incident Light.

	Angle		
	$\theta_a = 0^\circ$	$\theta_a = 15^\circ$	$\theta_a = 30^\circ$
Calculated Thickness (Actual: 3000 nm)	3089.18 nm	3139.11 nm	2932.5 nm
Percent Error	2.97%	4.64%	2.25%
Calculated Thickness (Actual: 6000 nm)	6178.36 nm	5929.43 nm	6212.43 nm
Percent Error	2.97%	1.18%	3.54%
Calculated Thickness (Actual: 12000 nm)	12356.7 nm	12207.7 nm	12059.4 nm
Percent Error	2.97%	1.73%	0.495%

Our percent error in each trial is significantly less than the established goal of 6%.

Accounting for a Conical Spread in Incident Light

To analyze the data collected by our exposure tool, we must consider the nature of our focused light beam. As illustrated by Figure 10, changing the angle of incidence appears to alter the periodicity of the reflectance spectrum as well as create a horizontal shift, which is not entirely compensated for by [II.18] due to the discrete nature of our FFT algorithm.

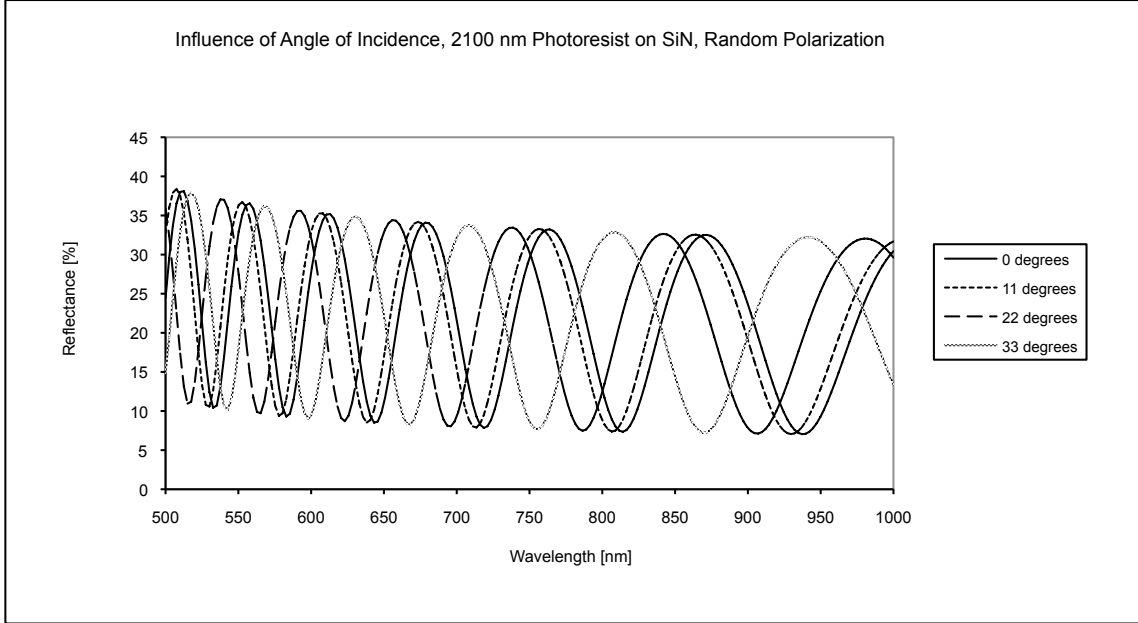


Figure 10. Angle of Incidence and Reflectance The reflectance spectrum for 2100 nm layer of photoresist is shown for differing angles of incident light. Note that there is a horizontal shift in the reflectance in addition to a change in periodicity.

The numerical aperture, NA , of the Mitutoyo 50x M Plan Apo Objective in our exposure tool is related to the maximum angle of incident light by the equation,

$$NA = n_a \sin \theta_{\max} . \quad [\text{III.1}]$$

We are given that $NA = 0.55$. Our ambient is air, so $n_a = 1$ and $\theta_{\max} \approx 33^\circ$. Thus, light will be conically incident upon the sample over an angular spread of 33° .

One hypothetical approach to account for the conical distribution of incident light would be to take a discrete, weighted average over the cone to construct an appropriate reflectance spectrum. For example, suppose we discretize the cone into two partitions according to angle. The average angle of incident light for a 33° cone is about 23° , i.e., 50% of the light is incident at less than the average angle. We could thus construct the reflectance spectrum by treating half of the emitted light at each photon energy or wavelength as incident at 23° and the other half as incident at 33° . In fact, we could construct two separate spectra, one for each angle of incidence, find the film thicknesses

suggested by the spectra with our FFT algorithm, and then average the two values. Going a step further, we could split the cone into as many partitions according to angle as signal strength will permit, and extend this same procedure for calculating thickness.

Figure 10 presents a significant challenge to this hypothetical approach. It is not clear how, without knowing the reflectance percentage at a specified angle of incidence, we could construct an appropriate reflectance spectrum from the measured data. Consider, for instance, 700 nm light incident on 2100 nm of photoresist on SiN. Looking at Figure 10, about 12% of incident light is reflected at 11° and 22° , 17% of incident light is reflected at 0° , and 32% is incident at 33° . Imagine an apparatus that emits light at only these four angles as follows: 40% is emitted at 33° , 30% is emitted at 22° , 20% is emitted at 11° , and 10% is emitted at 0° . Using the reflectance percentages given by Figure 10, we can predict that about 20.5% of the total light will be reflected. However, assume that we have no knowledge of the information contained in Figure 10; given only that 20.5% of the total light will be reflected, how are we then to deduce that 17% of our reflected light was originally incident at 0° ? Without knowing the reflectance percentages of light received at each of the four angles, such a calculation seems impossible. Our exposure tool does not preserve this vital information.

A suggested line of future research would be to approximate all light in the focused beam as incident at the average angle, 23° . If our accuracy goal of less than 6% error in thickness calculations is still met, there will be no need to further investigate how to account for the conical spread of incident light. On the other hand, if our accuracy goal is not met, modifications to our apparatus may need to be considered.

Also of concern is the loss of light inside the "Beam Shaping and Beam Steering" components of Figure 1, a more detailed view of which is displayed below in Figure 11.

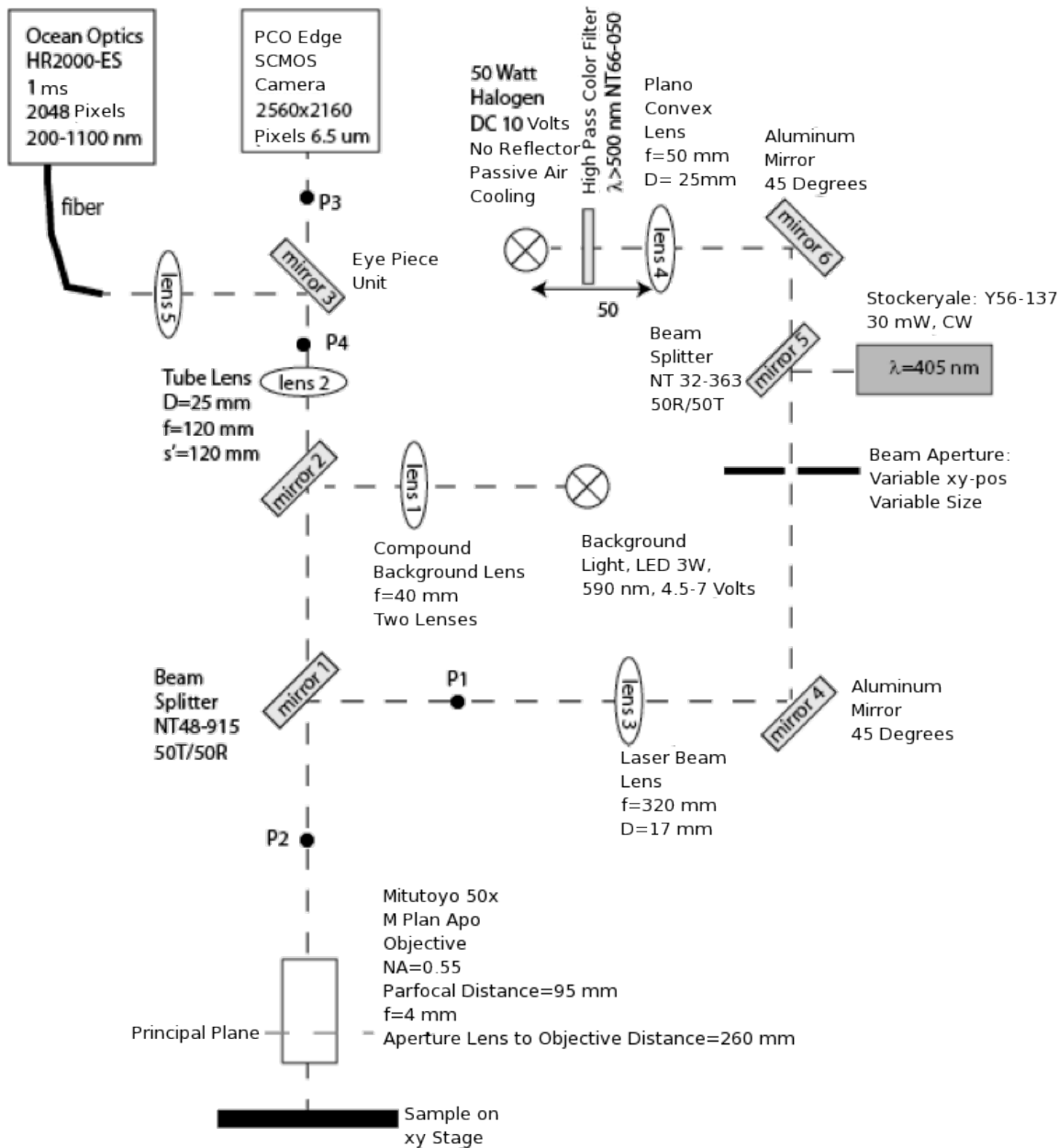


Figure 11. Beam Shaping and Beam Steering. The reflectance spectrum of the beam emitted by the halogen lamp is used to calculate film thickness, whereas the laser beam delivers an appropriate exposure dosage. The symbol D refers to the diameter of a lens, f to focal length, and s' to image distance.

Subsequent research should study how light intensity at each wavelength or photon energy is diminished by the transmission coefficients of the various lenses and mirrors in our exposure tool. We may need to modify our apparatus to maximize the light throughput of our system.

Noise Simulation

To simulate the noise expected in measurements obtained by our exposure tool, we originally planned to add white noise according to the following formula,

$$\text{noisy value} = \text{original} \left(1 + \frac{\text{rand}[\%]}{\sqrt{\text{original}}} \right), \quad [\text{IV.1}]$$

where $\text{rand}[\%]$ generates a random value ranging from $-\%$ to $+\%$ and $\%$ refers to the specified percentage of white noise. However, testing with 1000 trials indicated no effect on the accuracy of our FFT algorithm's thickness calculations even for noise percentages exceeding 350%. Therefore, we amended our noise model [IV.1] to

$$\text{noisy value} = \text{original}(1 + \text{rand}[\%]). \quad [\text{IV.2}]$$

The advantage of [IV.2] is that it represents a hybrid model between shot noise and other sources of noise such as dark current and read noise. Dark current refers to the small electric current present in a photosensitive device in the absence of photonic stimulation. CCD read noise is the result of on-chip imperfections and features. Shot noise is directly proportional to the square root of the flux of our halogen lamp and is dependent on wavelength. Dark current and read noise, however, are independent of wavelength.

We fixed our film thickness at 6000 nm and our angle of incidence at 15° , taking 1000 trials at steps of 25% white noise. Figure 12 shows the probability of obtaining a thickness measurement within 6% of the actual value for a given intensity of noise.

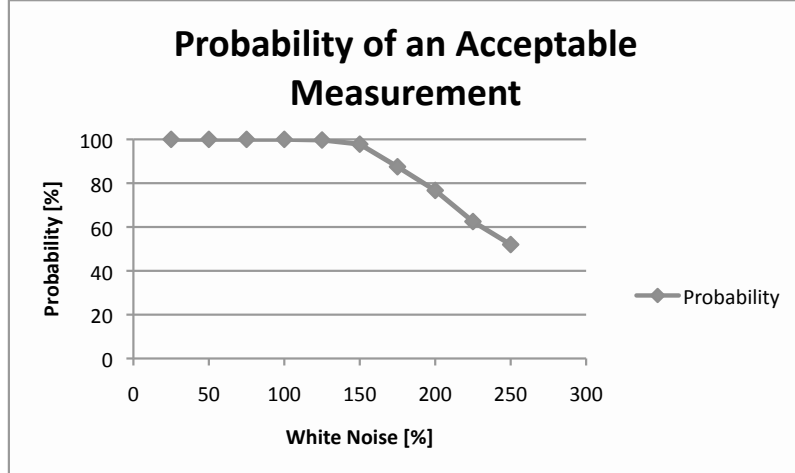


Figure 12. Probability of an Acceptable Measurement. The threshold of tolerable white noise intensity appears to be somewhere around 150%, however, we can extend this threshold by using previous measurements to assess the reasonableness of gathered data.

We demand that each measurement taken by our exposure tool has as close to a 100% probability of acceptability as possible. Our white noise threshold is thus approximately 150%. Methods that use multiple measurements might be able to extend this threshold. It is, however, an open question as to whether noise levels will ever exceed 150% and a possible subject of future research.

Preliminary Data and Conclusion

Our proof of concept for our FFT algorithm holds for exposure tools capable of preserving information about the angle at which reflected light is received in relation to the photoresist. Accuracy and time constraints have been met for simulated systems that emit light at a single angle of incidence. Moreover, the FFT algorithm has proven robust enough to handle up to 150% white noise.

It remains to apply our results to assess the feasibility of using the FFT algorithm with our non-standard exposure tool. Modifications to the apparatus, and to the

algorithm, may be necessary and are currently still a question of ongoing research. A preliminary reflectance spectrum obtained by our exposure device is shown in Figure 13.

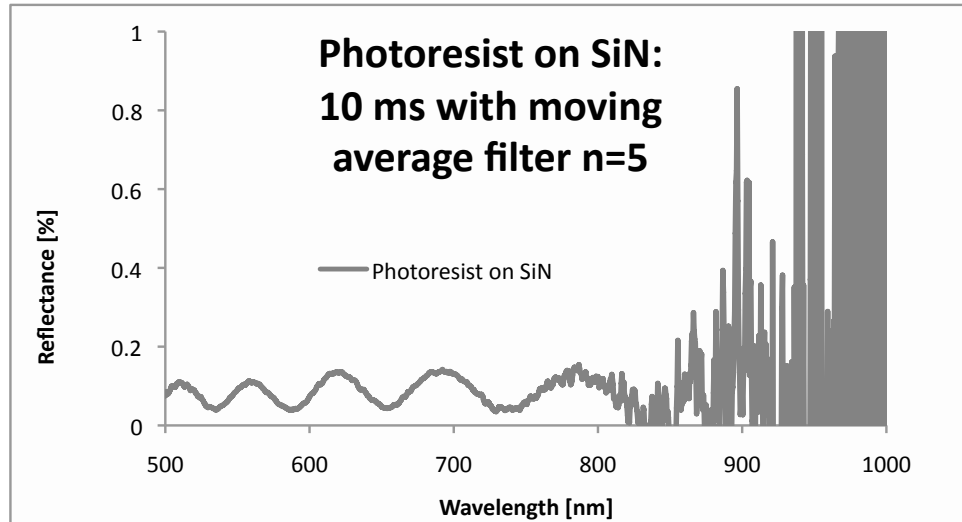


Figure 13. Preliminary Data. Our preliminary spectrum was constructed from measured reflectance data using a moving average filter of 5 data points. The thickness of Shipley S1813 sampled here is unknown.

The preliminary results show what appears to be an approximately uniform white noise distribution over the range 500 nm to 800 nm. For longer wavelengths, the noise levels increase significantly due to the lower halogen lamp intensity. Extrema are very clear from 500 nm to 800 nm. The next logical step in continuing research would be to format measurements for analysis by our FFT algorithm. Depending on the results from that study, other investigations, in particular the ones discussed during our data analysis, should be pursued.

APPENDIX A

PHOTORESIST DATA

The following pamphlet describes the properties of MICROPOSIT S1800 SERIES PHOTO RESISTS used for our research.



SHIPLEY

MICROPOSIT® S1800® SERIES PHOTO RESISTS

MICROPOSIT S1800 SERIES PHOTO RESISTS are positive photoresist systems engineered to satisfy the microelectronics industry's requirements for advanced IC device fabrication. The system has been engineered using a toxicologically safer alternative casting solvent to the ethylene glycol derived ether acetates. The dyed photoresist versions are recommended to minimize notching and maintain linewidth control when processing on highly reflective substrates.

MICROPOSIT S1800 SERIES PHOTO RESISTS FEATURE:

Product Assurance

- Lot-to-lot consistency through state-of-the-art physical, chemical and functional testing
- Filtered to 0.2 µm absolute

Coating Properties

- ¹Cellosolve® Acetate and xylene free
- Striation-free coatings
- Excellent adhesion
- Excellent coating uniformity
- A variety of standard viscosities are available for single-layer processing

Exposure Properties

- Optimized for G-Line exposure
- Effective for broad-band exposure
- Reflective notch and linewidth control using dyed versions

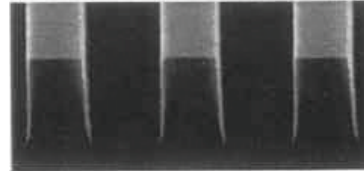
Develop Properties

- Optimized for use with the MICROPOSIT® MF®-319 Metal-Ion-Free DEVELOPER family
- Compatible with Metal-Ion-Bearing MICROPOSIT DEVELOPERS

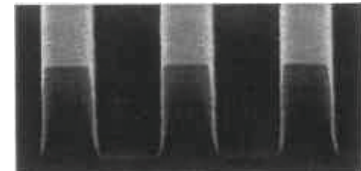
Removal Property

- Residue-free photoresist removal using standard MICROPOSIT REMOVERS

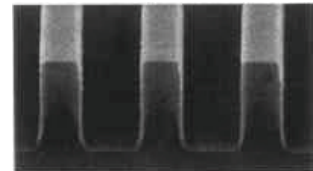
High Resolution Process Parameters (Refer to Figure 1)	
Substrate:	Polysilicon
Photoresist:	MICROPOSIT® S1813® PHOTO RESIST
Coat:	12,300Å
Softbake:	115°C/60 sec. Hotplate
Exposure:	Nikon 1505 G6E, G-Line (0.54 NA), 150 mJ/cm ²
Develop:	MICROPOSIT® MF®-321 DEVELOPER 15 + 50 sec. Double Spray Puddle (DSP) @ 21°C



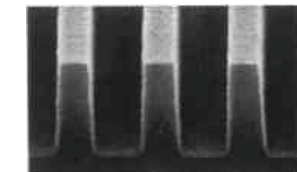
0.80 µm Lines/Spaces



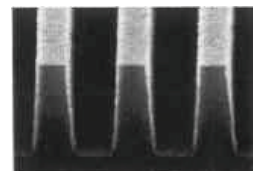
0.70 µm Lines/Spaces



0.60 µm Lines/Spaces



0.50 µm Lines/Spaces



0.48 µm Lines/Spaces

**Masking Linearity SEMS
Figure 1.**

¹Registered trademark of Union Carbide Corporation

Instructions for Use

The following instructions cover the use of MICROPOSIT S1800 SERIES PHOTO RESISTS for all levels of microelectronic device fabrication. Exact process parameters are application and equipment dependent.

Substrate Preparation

MICROPOSIT S1800 SERIES PHOTO RESISTS work well with the hexamethyldisilazane based MICROPOSIT PRIMERS. Concentrated MICROPOSIT PRIMER is recommended when vacuum vapor priming. Diluted PRIMER is recommended for liquid phase priming applications.

Coat

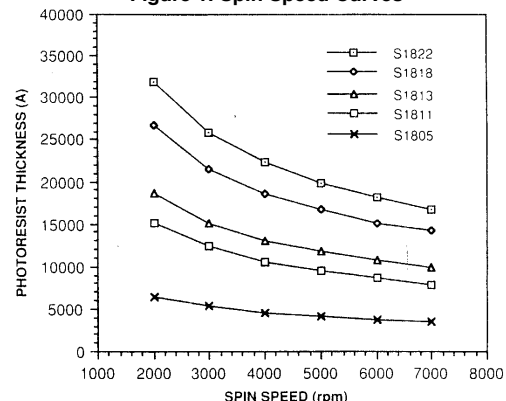
MICROPOSIT S1800 SERIES PHOTO RESISTS provide uniform defect-free coatings over a wide range of film thicknesses. The film thickness versus spin speed plots displayed in **Figures 1 and 2** provide the information required to properly select a MICROPOSIT S1800 PHOTO RESIST version to meet process dependent thickness specifications. Maximum coating uniformity is typically attained between the spin speeds of 3500 rpm and 5500 rpm.

Process Parameters (Refer to Figures 1 and 2)	
Substrate	Silicon
Coat	SVG 81
Softbake	115°C/60 seconds Hotplate
Measure	Nanometrics 210

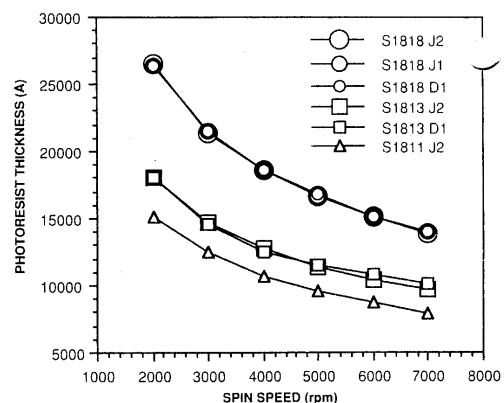
The dispersion curve and Cauchy equation displayed in **Figure 3** describe how the refractive index of the photoresist film varies as a function of the wavelength of light incident upon the film. This information is required to program ellipsometric and other optically based photoresist measuring equipment.

Process Parameters (Refer to Figure 3)	
Substrate	Silicon
Coat	13,675Å
Softbake	115°C/60 seconds Hotplate
Measure	Prometrix SM300

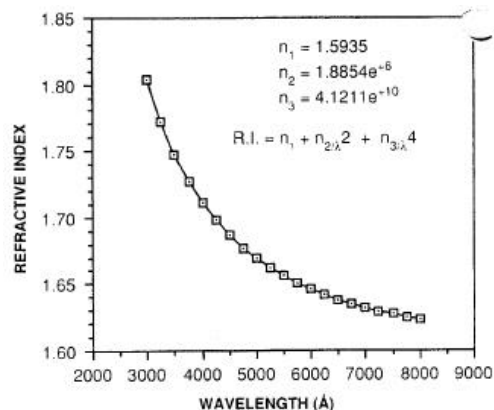
MICROPOSIT S1800 PHOTO RESIST UNDYED SERIES
Figure 1. Spin Speed Curves



MICROPOSIT S1800 PHOTO RESIST DYED SERIES
Figure 2. Spin Speed Curves



MICROPOSIT® S1813® PHOTO RESIST
Figure 3. Dispersion Curve



Exposure

Proper film thickness selection is critical in order to reduce photospeed and critical dimension variability. The interference curves displayed in **Figure 4** illustrate the photospeed variability as a function of film thickness. Dyed versions suppress the interference effects which are more pronounced when exposing with monochromatic light sources and when using reflective substrates.

Process Parameters (Refer to Figure 4)	
Substrate	Silicon
Coat	GCA 1006 ² WAFERTRAC [®]
Softbake	115°C/60 seconds Hotplate
Expose	GCA 8500 G-Line (0.35 NA)
Developer	MF-321 /10 + 30 DSP @ 21°C

MICROPOSIT S1800 SERIES PHOTO RESISTS can be exposed with light sources in the spectral output range of 350 nm -450 nm. The exposure properties have been optimized for use at 436 nm. **Figures 5 and 6** show the absorbance spectrums for MICROPOSIT S1813 and S1813 J2[®] PHOTO RESISTS.

Process Parameters (Refer to Figures 5 and 6)	
Substrate	Quartz
Coat	12,300Å
Softbake	115°C/60 seconds Hotplate
Expose	Oriel Scanning Wedge
Measure	Hewlett Packard 8450A Spectrophotometer

Table 1 summarizes the Dill parameters for each MICROPOSIT S1800 SERIES PHOTO RESIST version. Dill parameters are used in optical exposure models such as SAMPLE and PROLITH.

MICROPOSIT S1800 SERIES PHOTO RESISTS

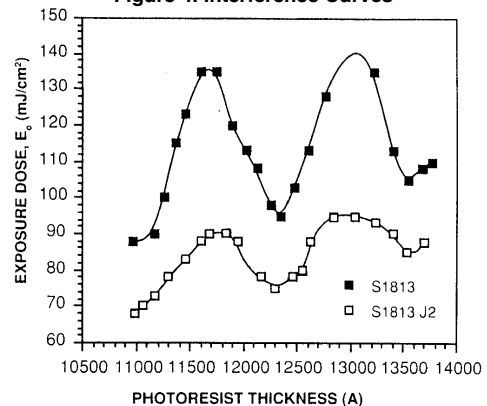
Table 1. Dill Parameters

Photoresist	365 nm		436 nm	
	A (μm^{-1})	B (μm^{-1})	A (μm^{-1})	B (μm^{-1})
S1813	1.07	0.31	0.61	0.08
S1813 D1	1.05	0.34	0.58	0.26
S1811 J2	1.07	0.49	0.59	0.61
S1818 J1	1.06	0.42	0.57	0.37

² Registered Trademark of GCA, a unit of General Signal

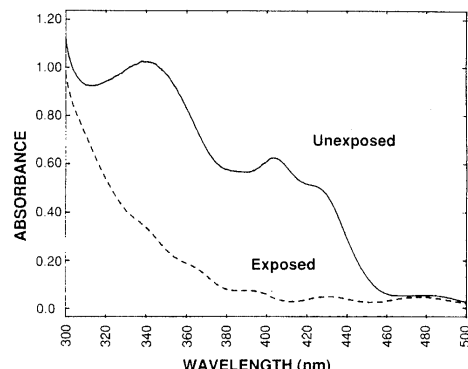
MICROPOSIT S1813 and S1813 J2 PHOTO RESISTS

Figure 4. Interference Curves



MICROPOSIT S1813 PHOTO RESIST

Figure 5. Absorbance Spectrum



MICROPOSIT S1813 J2 PHOTO RESIST

Figure 6. Absorbance Spectrum

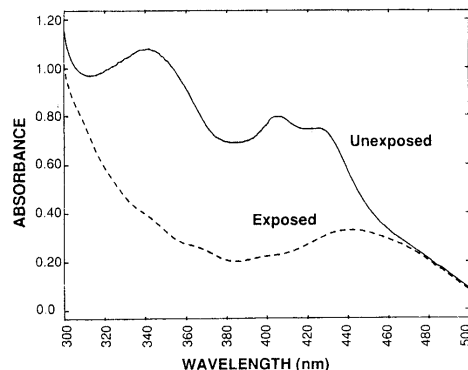


Figure 7 displays a contrast curve for MICROPOSIT S1813 PHOTO RESIST developed with MICROPOSIT® MF®-321 DEVELOPER. In general, high contrast values correlate to higher angle wall profiles.

Process Parameters (Refer to Figure 7)	
Substrate	Silicon
Coat	12,300Å
Softbake	115°C/60 seconds Hotplate
Expose	GCA 8500 G-Line (0.35 NA)
Develop	MF-321 /10 + 30 DSP @ 21°C

DEVELOP

MICROPOSIT S1800 SERIES PHOTO RESISTS are compatible with both Metal-Ion-Free (MIF) and Metal-Ion-Bearing (MIB) developers. A photoresist and developer system is dependent upon specific application requirements. Contact your local Shipley Technical Sales Representative for additional product information.

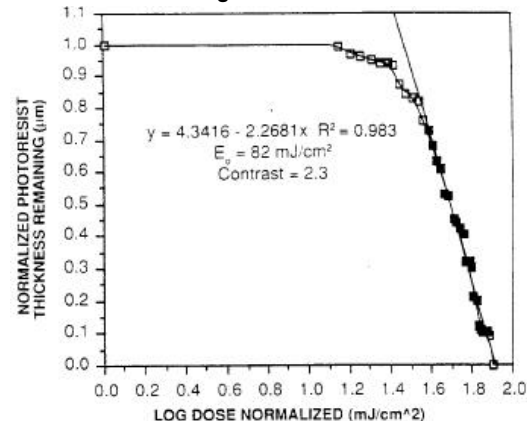
Figures 8 thru 10 illustrate the lithographic functionality of MICROPOSIT S1813 PHOTO RESIST using process parameters designed to maximize resolution while maintaining excellent exposure and focus latitude (refer to SEM photographs in **Figure 1**). The functional lithographic responses are summarized in **Table 2**.

Process Parameters (Refer to Figures 8 thru 10)	
Substrate	Silicon
Coat	12,300Å
Softbake	115°C/60 seconds Hotplate
Expose	Nikon 1505 G6E G-Line (0.54 NA)
Develop	MF-321 /15 + 50 DSP @ 21°C

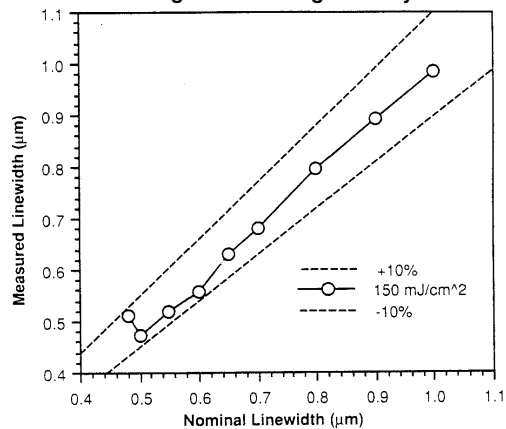
**MICROPOSIT S1813 PHOTO RESIST
with MICROPOSIT MF-321 DEVELOPER**
Table 2. Functional Lithographic Summary Data

Sizing Energy	150 mJ/cm ² (1.3 E ₀)
Resolution	0.48 µm
Masking Linearity ($\pm 10\%$ CD)	0.50 µm
	1.0µm L/S 0.60 µm L/S
Exposure Latitude ($\pm 10\%$ CD)	65% 45%
Focus Latitude ($\pm 10\%$ CD) $\geq 85^\circ$ Wall Angle	2.25 µm 1.25 µm

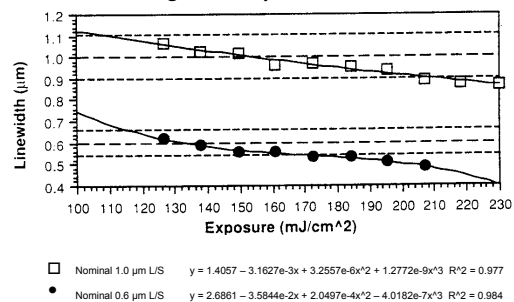
MICROPOSIT S1813 PHOTO RESIST
Figure 7. Contrast Curve



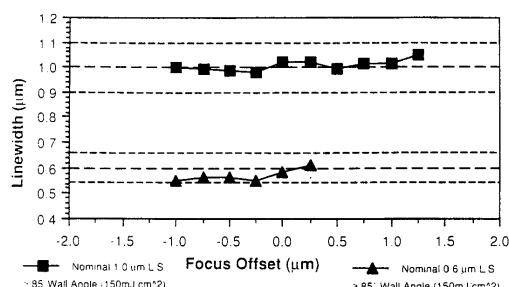
MICROPOSIT S1813 PHOTO RESIST
Figure 8. Masking Linearity Plot



MICROPOSIT S1813 PHOTO RESIST
Figure 9. Exposure Latitude Plot



MICROPOSIT S1813 PHOTO RESIST
Figure 10. Focus Latitude Plot



Equipment

MICROPOSIT S1800 SERIES PHOTO RESISTS are compatible with most commercially available photo-resist processing equipment. Compatible materials include stainless steel, glass, ceramic, unfilled polypropylene, high density polyethylene, polytetrafluoroethylene, or equivalent materials.

Technical Literature

Please contact your Shipley Technical Sales Representative for information on the use and performance of Shipley products.

Handling Precautions

WARNING: MICROPOSIT S1800 SERIES PHOTO RESISTS are combustible mixtures containing propylene glycol monomethyl ether acetate. Contact with eyes, skin and mucous membranes causes irritation. Handle with care. Do not get in eyes, on skin or on clothing. Avoid breathing vapors or mists. Use with adequate ventilation. Wash thoroughly after handling.

Wear chemical goggles, chemical gloves and suitable protective clothing when handling MICROPOSIT S1800 SERIES PHOTO RESISTS.

In case of eye or skin contact, flush affected areas with plenty of water for at least 15 minutes. Then contact a physician at once.

Consult product Material Safety Data Sheet before using.

Toxicological and Health Advantages

The solvent used in MICROPOSIT S1800 SERIES PHOTO RESISTS is propylene glycol monomethyl ether acetate. Toxicological studies reported that propylene glycol derivatives contained in MICROPOSIT S1800 SERIES PHOTO RESISTS do not demonstrate the adverse blood effects and reproductive effects that ethylene glycol derived ether acetates demonstrate (NIOSH Current Intelligence Bulletin 9-5/2/83).

Storage

Store MICROPOSIT S1800 PHOTO RESISTS only in upright, original containers in a dry area at 50°-70°F (10°-21°C). Store away from light, oxidants, heat, and sources of ignition. Do not store in sunlight. Keep container sealed when not in use.


Worldwide Operations

Shipley Company
455 Forest Street
Marlborough, MA 01752-3001
TEL: (508) 481-7950
FAX: (508) 485-9113

European Operations

Shipley Europe Ltd.
Herald Way
Coventry CV3 2RQ
United Kingdom
TELEX: 851311316
TEL: 441 203 457 203

Far East Operations

Shipley Far East Ltd.
Nishidai-NC Bldg.
1-83-1, Takashimadaira
Itabashi-ku, Tokyo 175
Japan
TELEX: 781 28875
TEL: 81 35 920 5300

Domestic Sales Offices

Marlborough, MA
(508) 481-7950
(800) 832-6200

Carrollton, TX
(214) 446-2400
(800) 527-3730

Tempe, AZ
(602) 894-5499
(800) 262-6377

Santa Clara, CA
(408) 988-3600
(800) 423-9937

International Sales Offices

Evry, France
33 1 60 86 81 82

Milano, Italy
39 2 938 1586

Geldrop, The Netherlands
31 40 853 335

Norrkoeping, Sweden
46 11 108170

Jona, Switzerland
41 55 284 646/647

Esslingen, Germany
49 711-931 32-0

Kowloon, Hong Kong
852 6 940 661

Singapore
65-862-1888

International Distributors

Australia, China, India, Israel, Mexico, Singapore, South Africa, South Korea, Spain, Taiwan, Western Canada.

Manufacturing Locations

Marlborough, MA; Coventry, United Kingdom; Sasagami, Japan.



For Industrial Use Only This information is based on our experience and is, to the best of our knowledge, true and accurate. However, since the conditions for use and handling of products are beyond our control, we make no guarantee or warranty, expressed or implied, regarding the information, the use, handling, storage or possession of the products, or the application of any process described herein or the results sought to be obtained. Nothing herein shall be construed as a recommendation to use any product in violation of any patent rights.

REFERENCES

- Doyle, William. 1980. Graphical Approach to Fresnel's Equations for Reflection and Refraction of Light. *American Journal of Physics* 48: 643-647.
- Jackson, John David. 1999. *Classical Electrodynamics*. 3rd ed. Hoboken, NJ: John Wiley & Sons.
- Sakurai, Jun, and Jim Napolitano. 2011. *Modern Quantum Mechanics*. 2nd ed. New York: Pearson/Addison-Wesley.
- Schatzman, Michelle. 2002. *Numerical Analysis: A Mathematical Introduction*. Trans. John Taylor. Oxford: Clarendon Press.
- Sauer, Timothy. 2006. *Numerical Analysis*. Boston: Pearson/Addison-Wesley.
- Tolstov, Georgi. 1976. *Fourier Series*. Richard Silverman. New York: Dover Publications.
- Tompkins, Harland, and William McGahan. 1999. *Spectroscopic Ellipsometry and Reflectometry: A User's Guide*. New York: John Wiley & Sons.
- Vogel, Curtis. 2002. *Computational Methods for Inverse Problems*. Philadelphia: Society for Industrial and Applied Mathematics.

VITA

Geoffrey F. Miller was born in El Paso, Texas, during 1988, the son of Carl and Gail Miller. After completing the International Baccalaureate Programme at L.C. Anderson High School, Austin, Texas, in 2006, he entered Texas State University-San Marcos. He received the degree of Bachelor of Science from Texas State in August 2009 with a major in mathematics and a double minor in computer science and honors studies. In August 2009, he was also received into the Graduate College of Texas State to pursue the degree of Master of Science with a major in mathematics and a minor in physics. During the summer of 2010, Geoffrey researched Lie Algebras with Dr. Thomas M. Keller for the math department at Texas State. From June 2010 to April 2012, Geoffrey worked as a graduate research assistant under Dr. Wilhelmus J. Geerts for the physics department at Texas State. Geoffrey's research focused on developing photolithographic approaches to photoresist deposits on non-flat substrates. Part of his work was presented at the spring 2011 meeting of the Texas Section of the American Physical Society in Nacogdoches at Stephen F. Austin State University. In March 2012, he was accepted into the Mathematics Education Doctoral Program, also at Texas State.

Permanent Email: miller.geoffrey@gmail.com

This thesis was typed by Geoffrey F. Miller.